# Experimental delta formation in crater lakes and implications for interpretation of Martian deltas

Germari de Villiers,[1] Maarten G. Kleinhans,[1] and George Postma[1]

Received 21 January 2013; revised 6 March 2013; accepted 6 March 2013; published 10 April 2013.

[1] The morphology of delta deposits in crater lakes on Mars is indicative of upstream (e.g., flow discharge and sediment properties) and downstream (e.g., basin characteristics) parameters, from which the hydrological conditions at the time of formation can be inferred. To investigate the influences of these parameters on delta morphology, we experimentally created deltas in crater-shaped basins by feeding a range of constant flow discharges over a feeder channel of various sand textures. We reproduced three categorically different types of deltas including most of the types that have been identified on Mars. Our most striking observation is that water level behavior (itself a unique function of flow discharge, basin size and hypsometry, and basin floor permeability) can explain most delta morphologies observed on Mars. Stepped, retrograding deltas formed during water level rise, prograding deltas formed during water level still stand, and during water level fall deltas were partially destroyed by erosion. On Mars numerous retrograding and prograding deltas were preserved, most of them without indications of channel incisions or other fluvial modification. We conclude that the main difference between a single-foreset prograding delta and a multiple-foreset retrograding delta is the behavior of the water level in the basin. These simple delta morphologies cannot be reconciled with long-duration hydrological activity, because that would imply crater lake fluctuations due to inherent complex water level histories along with complex sediment delivery histories. Our experiments and numerical verifications demonstrate that such deltas preferentially form during one aqueous event, which parsimoniously argues for short-duration hydrological activity.

**Citation:** de Villiers, G., M. G. Kleinhans, and G. Postma (2013), Experimental delta formation in crater lakes and implications for interpretation of Martian deltas, *J. Geophys. Res. Planets 118*, 651–670, doi:.10.1002/jgre.20069.

## 1. Introduction

[2] The presence of water on the surface of Mars is reflected throughout its history by the occurrence of large valley networks, regional outflow channels, and small, local gullies [e.g., *Carr*, 1983; *Cabrol and Grin*, 2001; *Gulick*, 2001; *Baker*, 2001; *Hynek et al*., 2010]. The occurrence of valley networks imply the possibility of rainfall in either a warm and wet surface environment [e.g., *Craddock and Howard*, 2002], or on the other hand a cold and dry surface environment with episodic floods [e.g., *Gaidos and Marion*, 2003]. Morphologies of sediment bodies within impact craters have been identified as alluvial fans and deltas [e.g., *Malin and Edgett*, 2003; *Irwin et al*., 2005; *Kraal et al*., 2008; *Hauber et al*., 2009; *Di Achille et al*., 2006] (Figure 1). The presence of deltas in craters implies that these craters were once water-filled (partially if not full) lakes early in Martian history [e.g., *Cabrol et al*., 2001]. As is known from Earth, delta morphologies contain information of the hydrological conditions that formed them. By analogy, Martian deltas may provide an indication of the hydrological conditions during the planet's history and contain valuable information about the magnitude and duration of fluid surface water.

[3] Terrestrial delta morphology is determined by upstream factors such as climate, geology, and vegetation, and by factors in the downstream receiving basin, such as basin morphology and subsidence, waves, tides, and sea level fluctuations [e.g., *Postma*, 1990, 2001; *Porebski and Steel*, 2006]. Because Martian deltas commonly formed in impact crater lakes with average diameters of around 40 km, waves were probably insignificant due to insufficient fetch distances and lower gravity [*Kraal et al*., 2006]. Tides were most likely absent because Mars has no large satellite like the Moon is for Earth. With no interference by vegetation on the surface of Mars, this leaves the upstream conditions (climate and sediment texture) and the downstream conditions (the dominant processes on the deltas and the behavior of the water level) as the most important formative parameters for deltas on Mars. Assuming that subsidence has likely played no role on Mars and thus could not have affected the behavior of the water level, we are discussing only water level changes related to the filling/draining of the basin.

[4] Climate variation affects fluvial sedimentation on different time scales [*Postma*, 2001] and can be a factor in

[1]Faculty of Geoscience, Utrecht University, Utrecht, The Netherlands.

Corresponding author: G. de Villiers, Faculty of Geoscience, Utrecht University, Heidelberglaan 2, 3584 CS, Utrecht, The Netherlands. (g.devilliers@uu.nl)


2169-9097/13/10.1002/jgre.20069

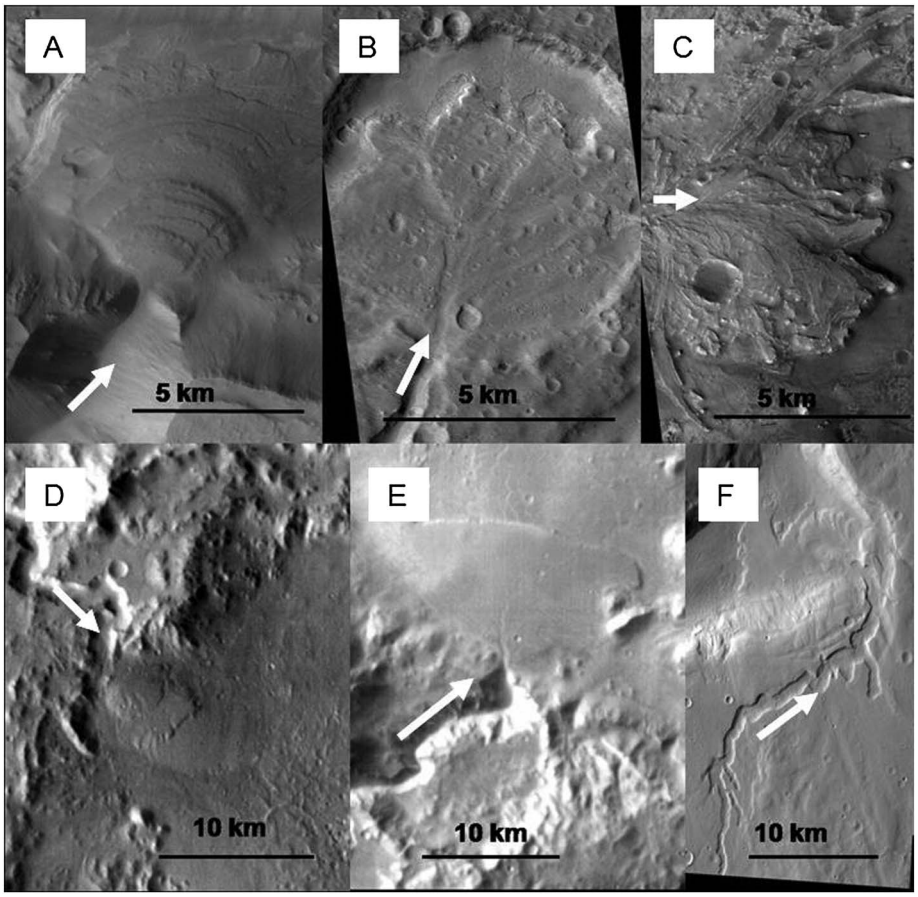


**Figure 1.** Examples of three categories of delta deposits on Mars formed in enclosed impact craters or rift basins. A and D) Multiple-scarped, stepped, retrograding deltas (THEMIS image V17040003 and I10125008). (B and C) Single-scarped, branched, prograding delta (HiRISE image PSP_006954 and PSP_003798). (E and F) Single-scarped, smooth, prograding delta (THEMIS image I10805012 and V12581003).

both the upstream and downstream environments. Previous experiments have demonstrated that delta morphology is particularly related to flow discharge and duration, sediment texture, and water level change [*Schumm et al*., 1987; *van Heijst and Postma*, 2001; *Muto and Steel*, 2004]. The same factors are expected to be important also on Mars, thus we focus on these in our experiments described below. In the upstream environment, source water generation can be highly sporadic thus producing large variations in runoff. This phenomenon could occur on either small or large time scales, for example short-term melting of ice or long-term stable rainfall. The amount of deposition not only depends on the amount of water but also on the sediment availability in the drainage basin, which may also depend on climate [*van Heijst et al*., 2001]. In the downstream environment, the water level behavior in a closed basin (like many of the craters on Mars) depends directly on the discharge (input rate) and partly on the rate of losses such as subsurface percolation and evaporation.

[5] The textural properties of the sediment, in particular grain size and grain sorting, determine the dominant transport processes and rate of delta formation. Grain size distributions are not well constrained on Mars, but *Kleinhans* [2005] suggests a coarse, bimodal sediment with particle sizes between 0.01 and 1 m for the gravel fraction and between 0.1 and 2 mm for the sand fraction based on rock size frequencies measured in Lander imagery [*Golombek et al*., 2003, *Herkenhoff et al*., 2004]. Given that Lander imagery has severe inadequacies such as poor representation of the natural spatial variability, limited resolution, sampling an armored surface, and underestimating the fines content due to shielding, we see these numbers as indicative. However, this kind of coarse sediment would still predominantly be transported as bed load [*Kleinhans*, 2005], which is associated specifically with steep sloping (~ 25°) delta foresets characterizing Gilbert-type deltas [*Postma*, 1990], also known as Gilbertian profiles. Deltas formed by suspended transport would have gentle (~ <1°) sloping foresets. The sediment on Mars is probably so poorly sorted that some of it is transported as bed load and some as suspended load, which could affect the morphology of the delta.

[6] Martian deltas exhibit many morphological elements that are similar to those of terrestrial deltas, e.g., fan shapes, surface gradients, concave/convex profiles, and presence of lobes and channels (see Figure 1 and Table 1). However, terrestrial deltas are not nearly as well-preserved or observable as deltas on Mars due to erosion and deformation, as caused by plate tectonics, climate and sea level changes, and vegetation. Moreover, some features of Martian deltas, for example the stepped profiles, are not commonly found on Earth. Based on

**Table 1.** Morphological Characteristics and Examples of Martian Delta Deposits [*de Villiers et al*., 2009]

| Approximate Shape | Multiple Foresets With Gilbertian Profiles | Single Foreset With Gilbertian Profile |
|---|---|---|
| Average Delta Plain Gradient | ~ 2 degrees | ~ 1 degree |
| Average Length | ~ 10 km | ~ 7 km |
| Example Locations | **−15.0°N 299.7°E** [*Di Achille et al*., 2006] **−10.9°N 306.6°E** [*Di Achille et al*., 2006] **8.3°N 310.7°E** [*Di Achille et al*., 2006b] | **−5.2°N 132.9°E** [*Irwin et al*., 2004] **8.5 N 312.0°E** [*Hauber et al*., 2009] **35.5°N 26.3°E** [*McGill*, 2002] |

a few simple morphological parameters like cross-sectional geometry and delta slope, most of the Martian deltas can tentatively be grouped into two categories, i.e., (1) retrograding deltas with multiple stacked steps of steep foresets of decreasing radius, and (2) prograding deltas with single steep foresets, either flat-topped or branched (Table 1) [*de Villiers et al*., 2009].

[7] Martian deltas have been considered in terms of location and environmental context and their formative processes inferred from general morphology [*Cabrol et al*., 2001]. Some studies have investigated the implications of observed delta locations and morphologies for climate conditions [e.g., *Di Achille and Hynek*, 2010], but these interpretations did not employ the full potential of laboratory experiments and numerical modeling on terrestrial and Martian deltas. Laboratory studies [e.g., *Muto and Steel*, 2001; v*an Heijst and Postma*, 2001; *van Heijst et al*., 2001] have shown that retrograding delta morphologies can be induced by climate-related base level oscillations. Numerical modeling studies [e.g., *Ritchie et al*., 2004] have also shown that base level oscillations produce distinct morphologies, most of which are clearly visible in both modern and ancient terrestrial deltas [e.g., *Tye and Coleman*, 1989; *van Heijst et al*., 2001]. Only one experimental study [*Kraal et al*., 2008] and one numerical study [*Kleinhans et al*., 2010a] were applied to Martian deltas, both suggesting that these deltas were formed in a single event, which is in stark contrast with the rich formative histories underlying many terrestrial deltas.

[8] Our objective is to systematically couple the simple morphological elements in Martian delta systems (see Figure 1) to their formative processes and boundary conditions through laboratory experiments. We test the hypothesis that the morphology of deltas on Mars and their (dis)similarities with their counterparts on Earth and in the laboratory are indicative of upstream (e.g., discharge amount and duration, sediment properties) and downstream (e.g., basin size and hypsometry) conditions at the time of formation. We focus particularly on deposits that exhibit steep peripheral scarps at their outer margins due to the interaction of the lacustrine regime and the water level in the receiving basin (often an impact crater). Specifically, our aims are to create various types of sedimentary deposits in the laboratory as a function of the aforementioned factors, to present both qualitative and quantitative evidence enabling us to relate formative processes and morphologies of the small-scale experimental deltas to the full-scale deltas on Mars, and to constrain the hydrological environment in which these deltas may have formed.

## 2. Experimental Methods

[9] The experimental work was carried out in the Eurotank facility at Utrecht University in the Netherlands. The Eurotank is a flume of 6.3 m wide, 11.4 m long, and 1.2 deep, within which sediment and water can be introduced to reproduce processes of erosion, transport, and deposition. Water was supplied by a regulated pressure tank, controlled by valves, and measured with rota-meters.

[10] We experimentally created deltas in small crater-shaped basins carved in sand. Various causal factors were isolated as much as possible by keeping most of the boundary conditions (e.g., discharge, sediment properties) constant and the initial conditions (basin morphology) idealized. We systematically varied one boundary condition, such as flow discharge or sediment properties and investigated the effect of crater basin size and shape. For each experiment we study rising, constant, and falling water level in the basin.

[11] The scaling approach of these landscape-sized models is the same as used by *van Dijk et al*. [2009, 2012] and *Kleinhans et al*. [2010b], where four criteria for flow and sediment transport characteristics are obeyed: (1) flow is fully turbulent, (2) flow is not above critical (Froude number $\leq 1$), (3) sediment is moved as bed load, and (4) the sediment must be coarse or poorly sorted enough to protrude the near-bed laminar flow layer, to ensure rough boundary conditions as to avoid the formation of small-scale ripples and unrealistic scour holes as observed in experiments by *Kraal et al*. [2008] and *van Dijk et al*. [2009]. The mobility of the sediment is determined mostly by channel gradient and depth. Depth on Mars is typically of the order of one to a few tens of meters [*Kleinhans et al*., 2010a], which would scale to one to a few millimeters in the experiment. To mobilize this sediment, the gradient thus must be much larger than in nature. Bed load movement by water flows in experimental set ups like ours requires slopes that are steeper than in nature, yet sediment mobility in experiment and in natural systems are comparable so that morphology is similar.

[12] Our setup was similar to that of *Kraal et al*. [2008], yet with a few modifications to both boundary and initial conditions (see Table 2). We constructed circular basins with diameters of 2 m (experiment numbers A-N) and 4 m (experiments O-S) with shapes comparable to those of complex impact craters. Martian complex craters have a diameter of more than 8 km and a flat crater floor (as opposed to simple, small, bowl-shaped craters; see *French* [1998] and *Melosh* [2011]), where the depth-diameter relation is a power function for pristine craters and where the idealized shape of the inner crater wall is also described by a power function [*Garvin and Frawley*, 1998; *Garvin et al*., 2000; *Kleinhans et al*., 2010a]. We modeled a crater of 40 km diameter without a central mound, which is the average size of craters with fan-shaped deposits. For the smaller crater a two times vertical exaggeration was applied to produce more pronounced deltas, while the larger crater was scaled with natural geometry. The crater depth as measured from floor to rim was about 15 cm in all cases.

[13] A feeder channel initially sloping 1.1° (± 0.4°) funneled water and sediment into the basin (Figure 2). Water discharge was systematically varied (Table 2) to obtain a range of crater filling rates and sediment mobility, and a range of ratios of crater diameter and self-formed channel

**Table 2.** Ten Sets of Experiments (Only First Phases) to Test Combinations of Flow Discharge, Particle Size Distributions, Silt Component, and Crater Diameter. Duration, Upstream Channel Slope, and Width Were Measured During Experiments. Delta Volume was Determined From DEMs and Modeled Volume was Calculated From Predicted Sediment Transport (see Text)

| Run | Basin Diameter (m) | Fines Content (%) | Grain Size ($D_{50}$) | Grain Size ($D_{90}$) | Discharge (L/s) | Time (H:M) | Average Slope | Width | Delta Volume (Actual) | Delta Volume (Model) |
|---|---|---|---|---|---|---|---|---|---|---|
| | | | (mm) | (mm) | | | (Dec) | (m) | (L) | (L) |
| A1 | 2 | 0 | 0.47 | 2.5 | 0.07 | 04:00 | n.d. | 0.168 | 7.6 | 97.7 |
| B1 | 2 | 0 | 0.47 | 2.5 | 0.21 | 00:30 | n.d. | 0.320 | 7.3 | 14.4 |
| C1 | 2 | 0 | 0.47 | 2.5 | 0.35 | 00:15 | 0.029 | 0.258 | 22.3 | 5.9 |
| D1 | 2 | 0 | 0.45 | 2.0 | 0.35 | 00:30 | 0.033 | 0.258 | - | 6.9 |
| E1 | 2 | 0 | 0.45 | 2.0 | 0.07 | 03:15 | 0.037 | 0.278 | - | 52.5 |
| F1 | 2 | 0 | 0.23 | 0.28 | 0.35 | 00:15 | 0.042 | 0.238 | 21.8 | 0.2 |
| G1 | 2 | 0 | 0.23 | 0.28 | 0.07 | 03:00 | 0.078 | 0.380 | 35.8 | 7.3 |
| H1 | 2 | 0 | 0.40 | 0.8 | 0.07 | 03:00 | 0.053 | 0.336 | 9.6 | 12.0 |
| I1 | 2 | 0 | 0.40 | 0.8 | 0.35 | 00:15 | 0.045 | 0.400 | 19.1 | 0.9 |
| J1 | 2 | 0 | 0.45 | 2.0 | 1.08 | 00:05 | 0.050 | 0.414 | 14.4 | 1.2 |
| K1 | 2 | 20 | 0.45 | 2.0 | 0.35 | 00:10 | 0.040 | 0.192 | 4.1 | 2.7 |
| L1 | 2 | 20 | 0.45 | 2.0 | 0.07 | 01:45 | 0.035 | 0.163 | - | 28.9 |
| M1 | 2 | 40 | 0.45 | 2.0 | 0.35 | 00:07 | 0.032 | 0.180 | - | 2.5 |
| N1 | 2 | 40 | 0.45 | 2.0 | 0.35 | 00:05 | 0.047 | 0.170 | - | 2.5 |
| O1 | 4 | 0 | 0.45 | 2.0 | 0.28 | 00:45 | 0.023 | 0.182 | 9.0 | 2.2 |
| P1 | 4 | 0 | 0.45 | 2.0 | 0.35 | 00:30 | 0.023 | 0.172 | 12.3 | 1.2 |
| Q1 | 4 | 0 | 0.45 | 2.0 | 0.07 | 03:45 | 0.017 | 0.163 | 7.7 | 9.1 |
| S1 | 4 | 0 | 0.45 | 2.0 | 0.35 | 00:30 | 0.020 | 0.200 | 15.4 | 48.3 |

width (which scales with discharge). In experiment J we applied the largest discharge possible with this setup. In experiment S we constructed a narrower feeder channel filled with sediment between nonerodible banks 0.25 m apart to investigate the influence of upstream channel dimensions on morphology.

[14] In all but two experiments, sediment for the delta became available through cannibalization of the feeder channel that widened and deepened during delta formation. In two experiments (F and G) sediment was added at the upstream boundary of the feeder channel. This mimics two possible sediment supply mechanisms on Mars, which is either a supply of sediment from a large upstream drainage area (here mimicked by feeding), or sediment delivered locally by headward erosion, widening, and some lateral migration of the feeder channel.

[15] Four sediment grain size distributions were applied to vary sediment mobility leading to bed load or suspended load-dominated sediment transport. We used three poorly sorted coarse sands (Sand 1 in experiments A-C, Sand 2 in experiments D-E and J-S, and Sand 3 in experiments H-I; see Table 2 and Figure 3) or uniform fine sand (Sand 4 in experiments F-G). By means of dry-sieving of the coarse tail of the sediment grain size distribution, the degree of size-selective transport and resultant spatial sorting patterns and armoring tendency found in Sand 1 in experiments A-C was reduced. The fraction greater than 4.7 mm was removed for experiments D and E as well as J-S, and the fraction

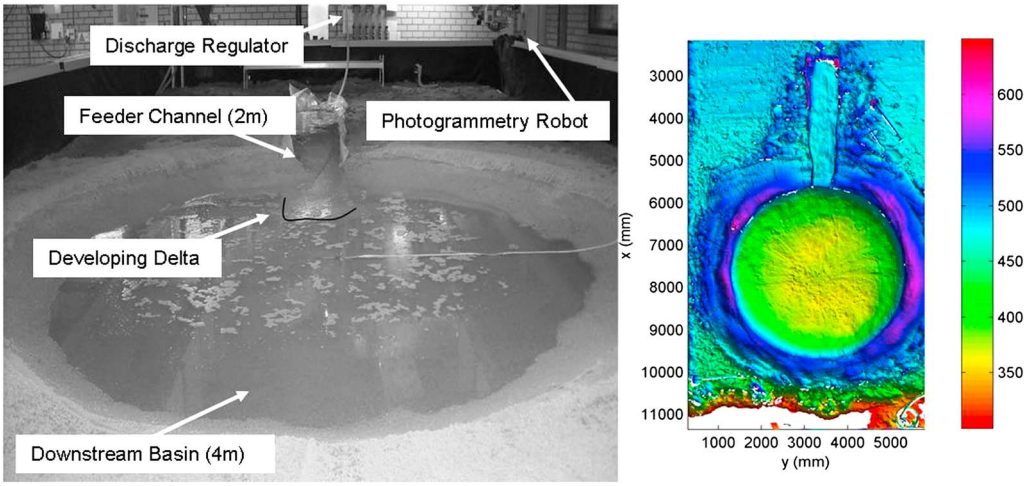


**Figure 2.** (left) Oblique photograph of the experimental setup in the Eurotank for run O with a filling lake and developing delta (looking upstream). The feeder channel is 2 m long and the downstream basin is 4 m wide (with foam floating on the water surface). (right) Shaded DEM of the unfilled crater with scales in mm.

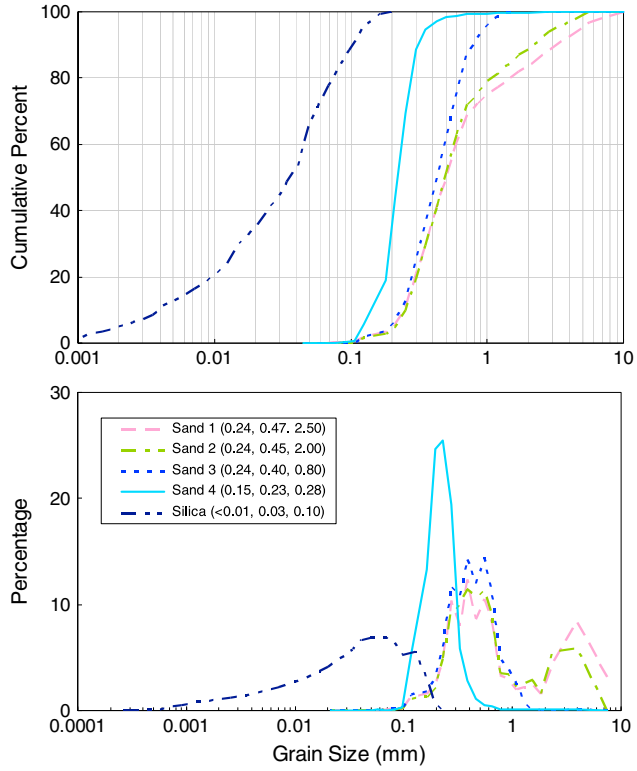


**Figure 3.** Sediment size distributions for the four different types of sediments and the silica flour used in the experiments (see full description in text). Sediment descriptions given as Sand type ($D_{10}$, $D_{50}$, $D_{90}$).

greater than 1.4 mm was removed for experiments H and I. The bed load to suspended load ratio was varied in experiments K-N by adding 20% or 40% by volume of silt-sized material (silica flour) in the feeder channel sediment (Table 2). Experiments with silica flour in concentrations higher than 40% resulted in undesired effects such as fluidized sediment transport and strong adhesive effects leading to hardening of the surface. This occurred due to complete filling of the pore spaces of the sand by the silica flour and a consequent decrease in porosity and permeability [e.g., *Kleinhans et al*., 2010b]. Silica flour was also added when molding the basin rim in some cases (experiments K-N) to reduce erodibility. In experiments M and N we tested the results of multiple drowning events, or in other words successive phases of filling and breaching of the crater. The only difference between M and N is that for experiment M we used full craters (craters filled with water up to the apex), whereas for experiment N we used half-full craters (craters filled only halfway before draining). This mimics a scenario where the breaching process occurs earlier (before the crater lake is filled up entirely and overflow occurs naturally) perhaps due to some inherent weakness of the crater rim. In fact, all our experiments are somewhat designed to occur like this because we always initiate breaching instead of waiting for overflow, but experiment N showed that even with only half-filled craters the delta morphologies remain similar.

[16] Each experiment listed in Table 2 was performed in two phases. In phase 1, the basin was filled with water through the upstream feeder channel. While basin level rose, sediment was supplied by a sediment feeder and/or eroded from the channel banks. Delta deposits were formed while the water level in the basin rose. Some water was lost by infiltration into the crater floor and wall. Once the basin was full, or when the water level reached the level of the feeder channel, we ended phase 1 and drained the crater to measure and photograph the delta deposit. Then we carefully filled the basin again to the former level and restarted the flow through the feeder channel before commencing with phase 2 and proceeding with manual breaching of the crater rim locally, to simulate water loss from the lake by overflow. This led to a constant water level in cases where water supply equaled discharge lost through the breach and into the subsurface, and otherwise to a fall in basin water level when the crater rim eroded rapidly. In every experiment discharge and sediment grain size distribution were kept constant.

[17] Morphology before, during, and after each experiment was measured through detailed photogrammetry using an automated positioning system designed for high-resolution surface scans. Digital elevation models (DEMs) for the 2 m craters were created from stereo pairs using the dedicated software SANDPHOX. DEMs for the 4 m craters were created from laser line scanning that was obtained after an upgrade of the laboratory equipment. DEMs were subsequently gridded and analyzed with median filtering for outlier removal to produce data similar to those taken by the High Resolution Stereo Camera onboard the Mars Express spacecraft.

## 3. Results

[18] All first phase experiments with rising water level produced retrograding or back-stepping deltas with lobes that stepped landward and did not fully cover previously deposited lobes as fan radius steadily decreased (Figures 4a and 4c). The experiments show that delta formation occurs by a sequence of events beginning with massive flows of relatively high sediment concentration gradually decreasing to dilute flow as the feeder channel decreases its slope with the filling of the lake. Initially, as the source water reaches the basin, the water first infiltrates through the permeable crater floor before starting to fill the crater. The first stage of fan formation is likely to be initiated by a hyperconcentrated particle flow or mass flow, which will deposit a fan-shaped drape on the crater wall. As water starts to pond, it begins to form a retrograding delta described in more detail below.

[19] During the second phase the crater rim was breached manually at a point causing water level to drop quickly as the unconsolidated rim eroded rapidly. This rapid lowering of the water level caused deep incisions in the fan surface and formed terraces and telescoping morphologies (Figure 4b). In the 4 m diameter crater with a wider rim, the outflow of water was relatively slower so that an almost-constant water level was maintained for some time. This resulted in the formation of well-developed, prograding deltas described in more detail below (Figure 4d).

[20] As a consequence of water level behavior in the crater lake, three main types of delta morphologies developed: (A) a retrograding, stepped delta morphology with multiple steep delta faces formed during rising water level

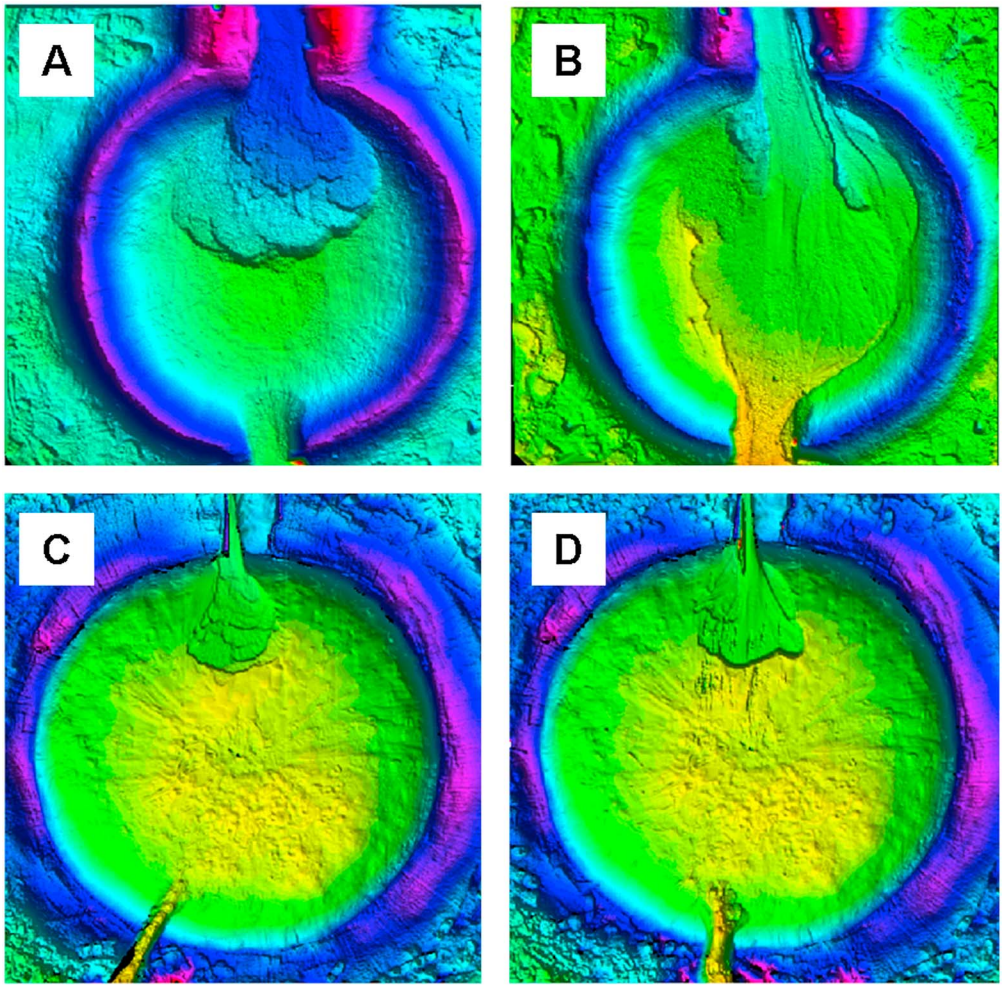


**Figure 4.** Shaded DEMs of deltas into constructed craters. (A and B) 2 m crater (run D); (C and D) 4 m crater (run P). Water and sediment enter from the top. (Figures 4A and 4C) Retrograding, back-stepping morphology as a result of basin level rise. Note that the crater rim was breached after the experiment to empty the lake to measure topography. Telescopic and incised prograding morphology as a result of rapid water level fall after breaching the crater wall; note terraces flanking the central channel (Figure 4B). Prograding morphology as a result of nearly constant basin level; note minor terraces flanking the central channel (Figure 4D). See DEM color bar in Figure 2.

(Figures 4a, 4c, and 5a); (B) a prograding delta morphology with a single steep delta face formed during constant water level (Figures 4d, 5b, and 5c), and (C) an incised delta with a telescoping morphology formed during falling water level (Figure 4b). We will call this large-scale or primary morphology.

[21] The profiles of both the retrograding and prograding deposits (Figure 6) demonstrate steep delta faces dipping about 25–27°, formed as a consequence of the predominant bed load transport [e.g., *Postma*, 1990]. The retrograding deposit profiles are distinctly stair-stepped with multiple, stacked, tabular delta bodies, whereas the prograding deposit profiles show only one continuous top-set and one delta face, much like a classic Gilbert-type delta. Each main type morphology deviates in detail (which we here refer to as secondary morphology) as a consequence of differences in water discharge and sediment texture. Deltas had more lobes during low discharge conditions and when poorly sorted sediment was used. We refer to the occurrence of more lobes as increasing lobateness, and we describe these variations in more detail below for the two experiment phases.

### 3.1. Phase 1: Rising Water Level

[22] In the initial phase of the experiment, the flow rapidly cut into the intersection of the crater and the upstream channel. The primary morphology of back-stepping or retrograding deltas was created mainly by the rising water level and all our phase 1 experiments showed similar primary morphologies due to this factor. Repeated bank collapse in the upstream channel is essential for the formation of back-stepping morphology, because the collapsed sediment temporarily enlarges the sediment flux to the delta. On a smaller scale, the retrograding deltas showed large variety in secondary delta morphology. Independent variables other than water level resulted in morphological elements that are superimposed on the primary, large-scale morphology. These independent variables are (1) discharge, (2) sediment texture

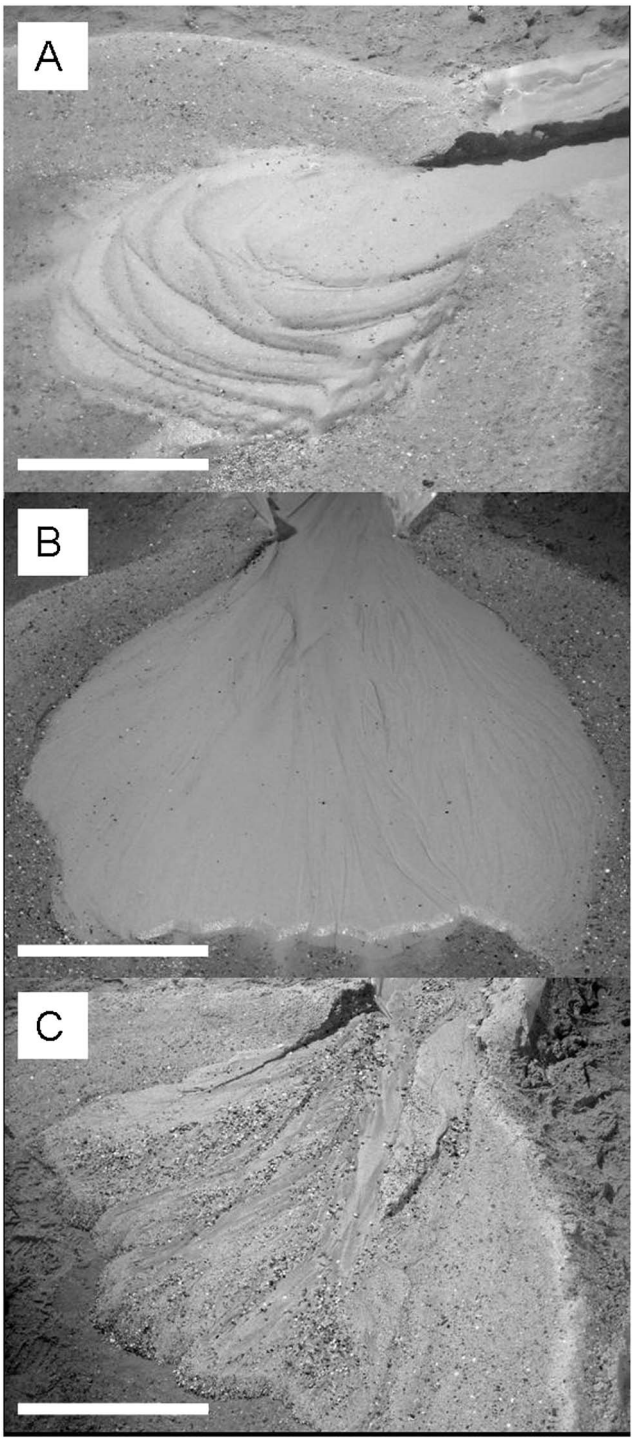


**Figure 5.** Examples of delta deposits in the laboratory. (A) Smooth, retrograding, stepped delta (run F); (B) smooth, prograding delta (run G); and (C) branched, prograding delta (run B). White line is ~50 cm.

(grain size and sorting) and percentage of suspended material, and (3) basin size and feeder channel width (Table 2).

[23] High discharge (0.35 L/s) showed much less channelization on the delta surface than low discharge (0.07 L/s) due to the wide sheet flow that dominated in these cases, and resulted in a more evenly distributed stepped delta with smooth edges (Figure 7a). On the other hand, lower discharge caused more and smaller lobes (Figure 7b). Low discharge experiments show channelization on the delta surface as flow focused in weakly defined channels that transported sediment to a segment of the shoreline. Nodal channel avulsion caused erratic, lobate stacking. In summary, a smaller discharge formed narrower channels that produced smaller lobes, and poorer sorting of the sediment caused more spatial sorting patterns that enhanced channelization, which also produced lobes.

[24] Coarser grain sizes (0.45 mm, poorly sorted) resulted in a more lobate delta shape and less well developed steps (Figure 7c). Finer grain sizes (0.225 mm, well sorted) resulted in a less lobate shape and better developed steps (Figure 7a; see trend in Figure 8). Clear sorting patterns were observed in the delta sets that were formed from the coarse and poorly sorted sediment. The top-set was coarse and often armored. The delta front was locally fining-upward but varied strongly spatially as each lobe and avulsion formed its own foreset. The toe-set consisted of very fine sand to silt that deposited from suspension, only when a significant amount of fine material was supplied to the system. This stratigraphic size-sorting is consistent with terrestrial Gilbert-type deltas. As can be expected, in the experiments with finer and well sorted sediment it was more difficult to observe clear sorting patterns. In some cases (e.g., experiment F) we observed a surprisingly regular pattern of increasingly smaller semicircles tabularly stacked one upon another (Figures 5a and 7a). Here we observed sheet flow rather than channelized flow, similar to the experiments of *van Dijk et al*. [2009].

[25] Deltas in the large 4 m crater basin experienced a much slower water level rise during phase 1 and fall during phase 2. Hence, the steps are fewer and the foresets are more pronounced (see Figure 7d) compared to those in the 2 m basins. Furthermore, as visible in Figure 7, the extent of the delta deposit is much less influenced by the physical crater rim boundaries for the bigger crater (Figure 7d) than for the smaller crater (Figures 7a, 7b, and 7c). In the small crater the delta deposit merges with the crater rim, while in the bigger crater the delta deposit does not, demonstrating that its fan-shaped morphology is unaffected by the crater rim. Hence, the ratio between the fluvial input and the size of the receiving basin might constrain delta morphology.

[26] Water loss occurred in the crater lake as a result of the permeability of the sand, especially during first event

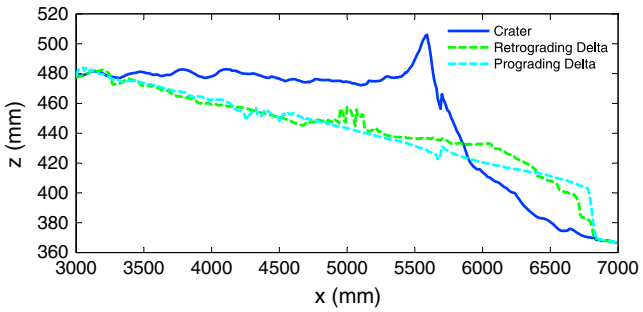


**Figure 6.** Long profiles of run P showing the difference in profiles of retrograding and prograding delta deposits. Flow is from left to right into the crater basin.

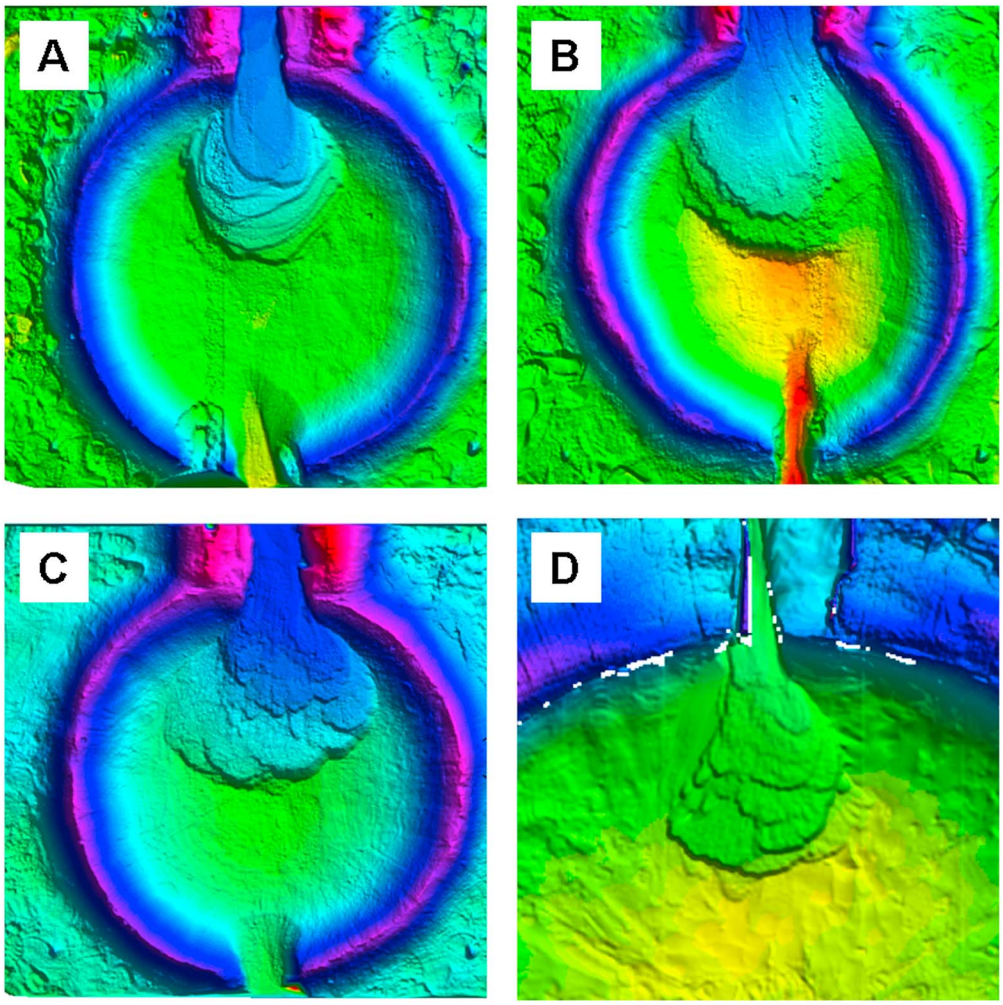


**Figure 7.** Shaded DEMs of four retrograding back-stepping deltas formed during rising base level conditions. (A) Run F (see Table 1) with high discharge, well-sorted fine sand in a small basin (2 m) showing a pancake stacking of lobes; (B) Run G with low discharge, well-sorted fine sand in a small basin (2 m); (C) Run D with high discharge, moderately sorted coarse sand in a small basin (2 m); and (D) Run P with high discharge, moderately sorted coarse sand in a large basin (4 m, also shown in Figure 4C). Vertical striping in Figures 7A and 7B is a minor DEM error made visible by the shading. See DEM color bar in Figure 2.

experiments (Figure 9). The ratio between the volume of water entering the crater ($V_{\text{water inflow}}$) and ponding water in the crater basin ($V_{\text{lake}}$) is in our experiments $V_{\text{waterinflow}}:V_{\text{lake}} \geq 1$. To obtain the minimum ratio of 1, we assumed that all lakes were filled at least 55% up to a lake depth of 8 cm. A different assumption will merely shift the data points up or down in Figure 9. Ideally the lake water level would have been measured during the experiments which could have led to somewhat different values, but we do not expect much difference between the assumed and true maximum lake level so the trend remains the same. Figure 9 demonstrates that for experiments of long duration a large amount of water up to a factor of 5 of the lake volume was lost into the subsurface through permeation. This occurred particularly when we used low discharge in long-duration experiments, because the amount of water that was added in each time step was small. This effect is much less obvious in the large crater lake experiments.

### 3.2. Phase 2: Constant and Falling Water Level

[27] Phase 2 experiments were initiated manually by creating a minor dent in the crater rim once the water level in the crater reached the current height of the mouth of the feeder channel that cuts through the crater wall. The breach never occurred at the 100% full level, but always at an earlier point as the feeder channel eroded into the crater rim while filling the crater. For the small crater, we estimate that the basin was usually about 80% full. For the large crater, we estimate that the basin was no more than 50% full. This difference between the small and large crater is likely a reflection of the fact that it took relatively much longer to fill the large crater than it took to fill the small crater (due to larger subsurface lateral discharge), and during that time the stream eroded more than halfway into the rim of the crater.

[28] Incision occurred regardless of the amount of discharge; however, we observed morphological differences in the incisions based on the amount of discharge. During the

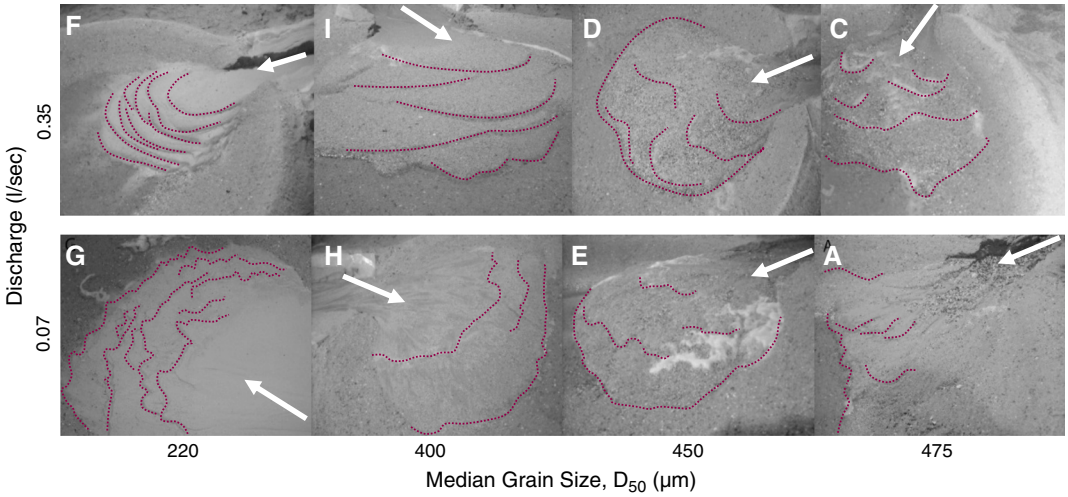


**Figure 8.** Photographs of eight retrograding back-stepping deltas formed during rising base level conditions in a small basin (2 m), showing an increase in lobateness with increasing grain size and decreasing sorting ($x$ axis) and decreasing lobateness with increasing discharge ($y$ axis). Flow direction is indicated by white arrows.

breaching event, the high discharge events created deeper incisions into the delta deposit than the low discharge events. For example, multiple channels were formed during low discharge, and a major single channel during high discharges (runs H and I respectively; Figures 10a and 10b).

[29] In both discharge cases the original stepped delta was partly eroded, but during high discharge much of the original deposit remains in the form of terraces raised about 2 cm above the channel elevation and the material that was eroded by this incising channel was reworked into a new delta (Figure 10b). The term "terrace" is used in this manuscript solely to refer to the erosional remnant that is left after a channel has incised a sedimentary deposit. The deltas in these experiments were generally dominated by erosion of higher parts of the deltas, and rapid deposition of the eroded sediment downstream of the deltas. When the water level fell rapidly, the water flow destroyed much of the original delta

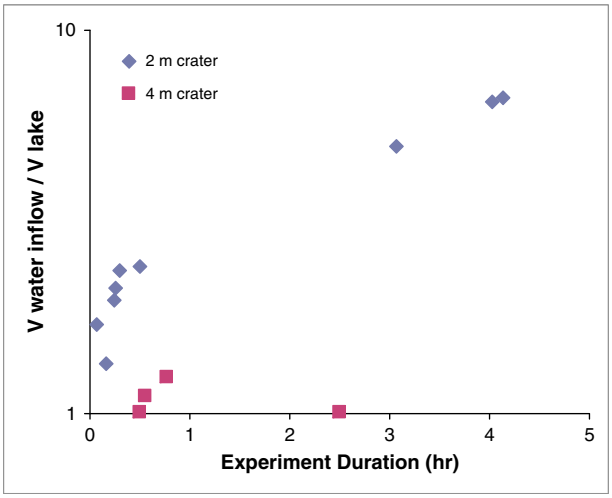


**Figure 9.** The water balance of the lake in phase 1 experiments, showing the ratio of real water inflow and final lake volume as a function of experimental duration.

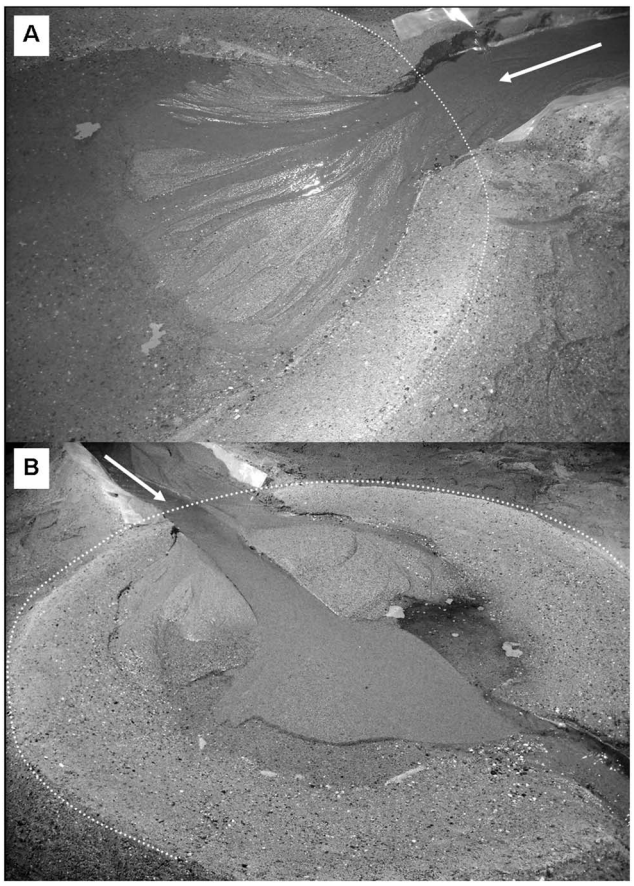


**Figure 10.** Different degrees of incision of the original delta deposit depending on the discharge. In A multiple channels incise in the delta plain (run H, 0.07 L/s), while in B a major channel incision occurs (run I, 0.35 L/s). Flow direction indicated by the white arrows and crater rim (2 m diameter) indicated by the white dots.

**Figure 11.** Thin layer of fine white sediment (silica flour) draped over the delta deposit and the crater floor (run L). Flow from right to left, with low discharge, and 20% volume percentage of silica flour mixed with sand.

body, and formed deep incisions flanked by terraces. Rapid incision caused rapid abandonment of the delta plain by funneling all the discharge through the incised valley. Especially in case of high (catastrophic) discharge (e.g., experiments D, F, I, but especially J), incision occurred very rapidly. Consequently less than 25% of the delta deposit by area was eroded by the self-confined incised channel, so that laterally more of the original deposit remained in the basin. During low discharge on the other hand, shallow incisions (e.g., experiments E, G, H) caused destruction of the delta across a larger area of the delta plain (Figure 10a) due to lateral channel migration without carving such deep incisions into the delta. Thus, lateral channel shift forced by low discharge is crucial in maintaining the development of a unified delta front after crater rim breach. Formation of large terraces on the delta surface (Figures 4b and 10b) could only be avoided if the discharge was low and the water level was constant for some time, i.e., the water left the basin at the same rate that it entered, whilst maintaining some ponding water in the basin. This was never completely the case in our experiments within the 2 m diameter crater because the crater rim continued to erode much faster than anticipated, even when cohesive materials was added to the gravelly river sand. However, in the 4 m craters the rim erosion was less abrupt and nearly constant water level was maintained in most of the phase 2 experiments. Hence, a more pronounced delta foreset developed, overprinting the less clearly stepped fan of phase 1. Minor erosion caused by high discharge created small terraces that flank the new channel (Figure 4d). In all cases where the water level fell while the lake was still fed, the delta deposit was incised.

[30] As in the phase 1 experiments, coarser grain sizes resulted in more lobes on the delta front. The poorly sorted sand and silica flour mix (experiments K-N) was eroded much slower in the upstream feeder channel. The silica flour was transported in suspension further into the basin than the sediment transported as bed load (Figure 11). The adhesive properties of the silica flour appeared not to have much effect on the erosion rate of the downstream crater rim (which was also constructed from poorly sorted sand with a percentage of silica flour), and thus water level dropped swiftly despite the extra adhesion. Additionally, almost no difference between 20% (experiment K) and 40% (experiment M) silica flour was observed in the erosion rates in the upstream feeder channel, on the fan itself, nor in the downstream breached crater rim.

[31] Lastly, we observed in experiment M that multiple filling and draining events leave distinct erosional signatures on the older delta plains and hence we can say with confidence that simple, stair-stepped morphologies can only have formed in one event.

## 4. Quantitative Approach

[32] Because laboratory results show that the formation of delta morphologies in crater-shaped basins are similar to delta morphologies found in some craters of Mars, and that these morphologies can be coupled in a simple way to discharge events and grain size, it is important to quantify the laboratory results to predict minimum duration of hydrological activity. This would further lead to predictions whether periods of wet climate are required on Mars or that short duration events would suffice for the formation of the Martian crater deltas.

[33] For Martian deltas we would want to know the dominant formative processes to infer the formative flow discharge and duration of the event or multiple events. One method to do this is by calculating volumes of the water and sediment bodies and dividing these by fluxes calculated from the upstream channel dimensions [*Kleinhans*, 2005]. In the experiments, the boundary conditions and formative duration were imposed and the dominant processes were observed. By using physics-based methods for calculation it should in principle be possible to combine small-scale experiments on Earth with full-scale prototypes on Mars. This requires that the proper processes at both scales are included. We will therefore combine the experiments with predictive calculations for two purposes: to assess scaling effects in the detailed flow and sediment transport processes, and to estimate relevant dimensionless parameters that allow application of our results to Martian systems.

[34] First, detailed flow and sediment transport processes that could not be measured in detail in the present setup are calculated. Flow discharge is controlled through the rota meters at the inlet, but velocity and depth measurement is deemed to be inaccurate in these shallow flows. The latter variables are nevertheless required to assess possible scale effects and calculate dimensionless parameters to be compared to those on Mars. We therefore present a method to calculate flow resistance in the laboratory.

[35] Second, the experimental data allow a basic proof of principle for the method used to calculate formative duration for Martian cases, which is sediment transport calculation from channel dimensions and formative duration estimation from deposit volume. We will also assess to what extent the standard prediction of sediment transport under-predicts the formative time scale taking in mind that there is an initial period of "en masse" sediment transport that is ignored in such predictors. We apply a sediment transport predictor for bed load appropriate for very steep slopes to predict slope development for a schematized experiment in a large

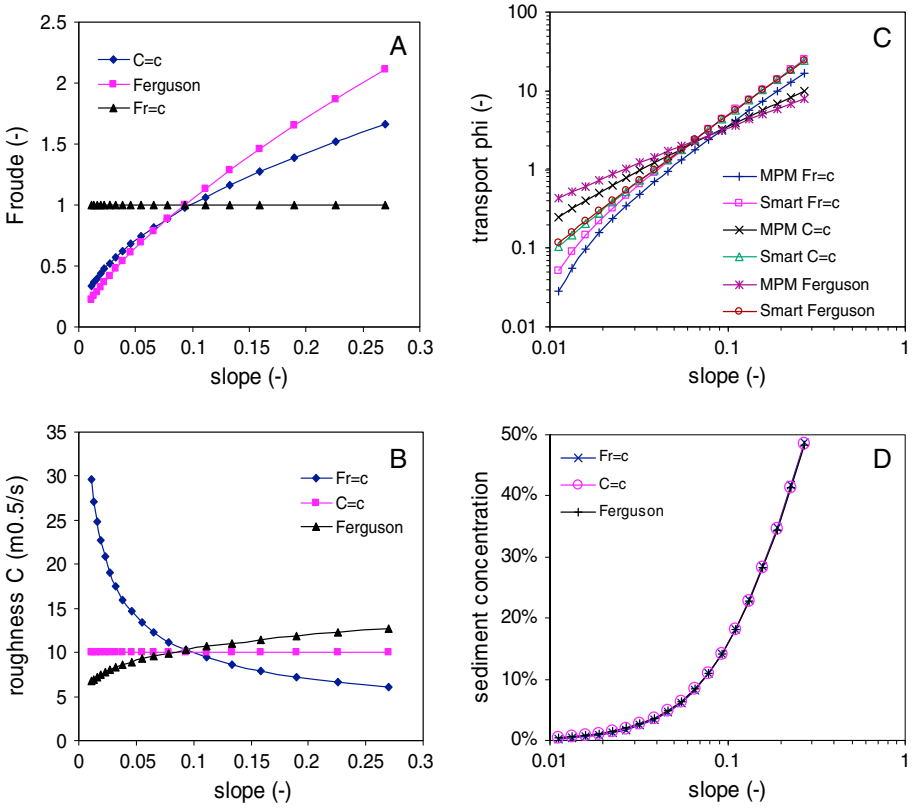


**Figure 12.** (A) Froude number (*Fr*) as a function of bed slope for three different assumptions for flow depth and velocity calculation where *Fr* is constant, *C* is constant or the resistance relation of *Ferguson* [2007] is used. (B) Chézy resistance coefficient (*C*) as a function of bed slope for the three different assumptions for flow depth and velocity calculation. (C) Dimensionless sediment transport rate as a function of bed slope for the *Meyer-Peter and Müller* [1948] sediment transport predictor (MPM) and the *Smart* [1984] predictor for the three different assumptions for flow depth and velocity calculation. (D) Volumetric sediment concentration in the flow as a function of bed slope for the *Smart* [1984] predictor for the three different assumptions for flow depth and velocity calculation.

crater to back-calculate the formative duration and the importance of hyperconcentrated flow in general.

[36] Finally, we apply the sediment transport prediction to the final measured conditions and compare predictions against measurements for all experiments to analyze the effect of both the underlying assumptions as well as the independent variables. The analysis will show whether the relevant dimensionless numbers are within the range of the calculated cases on Mars (reported in *Kleinhans et al.* [2010a]). In our quantitative analysis of sediment transport as observed in the experiments we will further discuss how to apply our findings quantitatively to Martian deltas.

### 4.1. Calculation of Flow Resistance

[37] Calculation of bed shear stress $\tau$ [N/m$^2$], the driving force per unit area for sediment transport, requires a water depth $h$ [m] and a gradient $S$ [m/m]

$$\tau = \rho g\, h \sin(S) \tag{1}$$

where $\rho$ is the density of water, here 1000 kg/m$^3$, and $g$ is the gravitational acceleration, here 9.81 m/s$^2$. In the experiment, the final channel slope was measured, the channel width $W$ [m] was measured and the flow discharge, defined as $Q = Whu$ where $u$ [m] is flow velocity, was set. This leaves the unit discharge $q = hu$ [m$^2$/s] known but the values of $h$ and $u$ unknown. For Martian conditions these can be calculated from a semiempirical friction relation [see *Kleinhans*, 2005], but for the shallow-flow experiments we must use a different approach. Three alternative assumptions about the relation between $h$ and $u$ are compared here.

[38] The first possible assumption is that the flow is critical with Froude number unity, defined as

$$Fr = u/\sqrt{(g\, h)} \tag{2}$$

[39] This condition is commonly found in natural gravel-bed rivers that are more or less in equilibrium [*Grant*, 1997]. Steeper slopes of rapidly incising channels are however known to become supercritical temporarily [*Cantelli et al.*, 2004].

[40] The second possibility is to assume that the flow resistance is constant, or $C = c$, where

$$C = \sqrt{(h\, S)}/u \tag{3}$$

according to the law of Chézy [*Rickenmann*, 1999, equation (A13)]. From this it follows that

$$Fr = C^2 S/g \tag{4}$$

[41] The third possible assumption is to use the empirically found flow resistance predictor of *Ferguson* [2007, equation (16b)], which was designed and calibrated for shallow gravel bed rivers over a large range of channel slopes:

$$C = (g)^{0.5}\,\alpha^{0.4}\left[q/\left(g(\mathrm{D}_{90})^{0.3}\right)^{0.5}\right]^{0.6} S^{0.2} \tag{5}$$

where α (an empirical fitting parameter) is in the range 1–4, here chosen as 2. It is noted that this friction coefficient $C$ does not include the extra friction due to high sediment concentration.

[42] In our flume experiments, the channel slope varied between 0.27 m/m, the slope at the first instant of flow when it entered the crater from the channel, and 0.01 m/m. We compare the Froude and Chézy numbers for the three assumptions along this range of slopes (Figures 12a and 12b). For $C = c$ and the Ferguson relation the Froude number decreases with decreasing slope from a high value ($Fr \sim 1.2$–$1.4$) where antidunes are stable [M. Cartigny et al., Morphodynamics and sedimentary structures of bedforms under supercritical-flow conditions: new insights from flume experiments, submitted to *Sedimentology*, 2013] and which we did observe in the experiments, to a rather low value for flat bed experiments where the $C = c$ assumption takes an intermediate position between the $Fr = 1$ and Ferguson assumptions. The Chézy number depends inversely on slope for the $Fr = 1$ assumption, and increases slowly with slope for the Ferguson predictor. The three assumptions have similar $C$ for $S \approx 0.1$. To summarize, the assumption of constant Chézy number leads to intermediate Chézy numbers and Froude numbers between the other two methods, so for the remainder of this paper we use $C = c$ for calculations on experimental data, thus following *Rickenmann* [1999].

### 4.2. Sediment Transport Rate

[43] Two predictors for sediment transport were used: the *Meyer-Peter and Mueller* [1948] (MPM) predictor and the *Smart* [1984] predictor. The MPM predictor is valid for bed load dominated transport and was successfully calibrated and tested in laboratory within a factor of 2–3 for the entire range from beginning of motion to high mobility [*Kleinhans and van Rijn*, 2002; *Wong and Parker* 2006]. Given the flat bed conditions in the experiments, total shear stress is used for transport prediction and no correction for form drag by bed-forms is applied. It was applied in the same manner to Martian deltas [*Kleinhans*, 2005; *Kleinhans et al*., 2010a]. MPM is calculated as

$$\varphi = 8(\theta - 0.047)^{1.5} \tag{6}$$

where θ is the Shields mobility number defined as

$$\theta = \tau/[(\rho_s - \rho)g\mathrm{D}_{50}] \tag{7}$$

where $\rho_s$ is the density of sediment, here 2650 kg/m$^3$. Dimensionless transport φ is defined as

$$\varphi = q_b/\left\{[(\rho_s - \rho)/\rho]g\mathrm{D}_{50}{}^3\right\}^{0.5} \tag{8}$$

where $q_b$ is the dimensional transport rate in m$^2$/s, which is m$^3$/s per m channel width.

[44] The Smart predictor is an extended version of MPM, which was empirically adapted for high concentrations and steep slopes nearly up to the angle of repose, and is formulated as

$$\varphi = 4.2S^{0.6}C\theta^{0.5}(\theta - \theta_c) \tag{9}$$

where is the critical Shields number for incipient motion, here taken at 0.047 for consistency with MPM.

[45] The prediction of transport rate is compared for all combinations of the two sediment transport predictors and the three assumptions for flow calculation (Figure 12c). For steep slopes $S > 0.06$, the Smart relation predicts higher transport rates than the MPM relation in all cases. For lower slopes, the Smart relation predicts rates intermediate between rates with MPM and $Fr = c$ on the lower end and MPM with $C = c$ and Ferguson on the higher end. The volumetric concentration of sediment in the flow for the Smart relation hardly depends on the assumption for flow behavior and is less than 5% for slopes $S < 0.05$. For channel slopes approaching the angle of repose the sediment concentration approaches that of unconsolidated sediment at rest. This behavior is expected as avalanching will occur at such angles with such concentrations.

[46] To summarize, the transport rate depends strongly on channel slope. The differences between the assumptions for the calculation of flow conditions are large but have a limited effect on the transport prediction. But the sediment transport rate may vary during formation and thus the effect of the time-dependent evolution of the eroding channel on the estimation of formative time scale based on the final slope must be investigated further.

### 4.3. Idealized Model for Linearly Decreasing Channel Slope With Time

[47] Formative duration is calculated from sediment transport rate and delta volume. For Martian cases the final channel morphology has to be used for flow and sediment transport calculation, but in the experiments we observed the initiation of the channels, including the transition from initial slope failure and hyperconcentrated flow to the dilute flow that is assumed in the predictors. Real formative time scale in the laboratory is accurately determined by the experimental duration, and the real volume of the deposited delta can accurately be measured from DEMs. The channel slope was only measured after the experiment, but was much steeper during the beginning of the experiment and gradually declined as the channel eroded. This was particularly the case in the vertically exaggerated crater experiments. Therefore,

**Table 3.** Initial Values for the Idealized Model Scenario

| Parameter | Value |
|---|---|
| Flow discharge [m$^3$/s] | $1.0\times10^{-4}$ |
| Channel width [m] | 0.1 |
| Initial slope [m/m] | 0.27 |
| Knickpoint depth [m] | 0.056 |
| Rim height [m] | 0.028 |
| Rim width [m] | 0.24 |
| $D_{50}$ of sediment [m] | $0.45\text{x}10^{-3}$ |
| $D_{90}$ of sediment [m] | $1.0\text{x}10^{-3}$ |

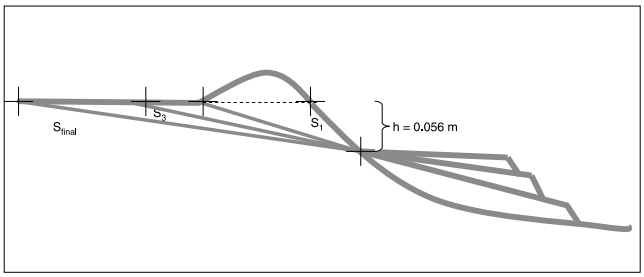


**Figure 13.** Schematic drawing of the back-cutting process that erodes sediment from the upstream channel and deposits this sediment as a delta in the downstream basin. Flow is from left to right. Compare to measured profiles in Figure 6. Specifically for run P, rim height is ~0.160 m, knickpoint height is ~0.087 m, rim width is ~0.180 m, knickpoint distance is ~2.670 m from flow starting point. The rim height and width add extra eroded sediment in the first phase of channel cutting. The slope of the eroding channel is assumed to be linear with an upstream knickpoint. The channel has a decreasing slope over time whilst it lengthens in upstream direction as the knickpoint migrates.

we can use the experimental data given in Table 3 to test the bias in the calculation of formative duration from final channel dimensions.

[48] As flow is transporting sediment, the channel feeding into the lake is eroded while the delta grows by deposition. The initial channel was very steep at the point where it entered the lake, but rapidly became gentler and longer as it eroded. For the estimation of formative time scale the final observable channel slope must be used because only that is observable [*Kleinhans*, 2005]. We investigated the effect of the time-dependent slope on the formative time scale estimate by an analytical method that is described in detail in Appendix A. The idea is to calculate the duration of erosion of a series of wedges as the channel cuts backwards. The underlying assumption is that the channel slope is straight, that the base of the channel remains fixed at some point on the crater wall, and that the flow can be calculated assuming $C = c$ and sediment transport can be calculated with *Smart* [1984].

[49] A logarithmically decreasing series of slopes is predefined to represent the back-cutting channel, where $S_1 = 0.27$ (the initial slope on the large experimental crater wall) and $S_{\text{final}} = 0.01$ (the final slope, which is the minimum of the observed final slopes in all experiments reported here). The cross-over point where the eroding channel becomes the delta deposit is the starting point for all measurements (Figure 13). Based on DEM values from experiment P, a difference in height of 0.056 m between the cross-over point and the original channel elevation is used. It may have varied in reality as the lake filled, while the channel cuts back, but this could not be measured. The height ($h$) and the slope together define the channel bed where channel length is calculated for each slope $S_i$ as $L_i = 0.056/S_i$ and the channel head is located at distance $L_i$ from the crater rim. Two subsequent slopes define an obtuse triangle of sediment (a sediment wedge), of which the surface area $A_i$ is calculated as $A_i = 0.056\ (L_i - L_{i-1})/\ 2$ where $(L_i - L_{i-1})$ is the length of the base of the obtuse triangle. The volume of eroded sediment for each step is $WA_i$. The time to erode this volume of sediment is calculated as detailed above, using a staggered scheme with slopes $S_{i:(i+1)}$ in between the slopes $S_i$ defining the obtuse triangle to better represent average conditions during the erosion of this segment.

[50] As expected from Figure 13, the time to erode the channel backward increases rapidly with decreasing slope (Figure 14a). Likewise, the knick-point or channel head migrates slower and slower as the experiment progresses and slope decreases. Consequently, a large fraction of the valley volume is eroded in a relatively short initial period of time that is characterized by very large transport rates (Figure 14b). From the increase of volume in the final stage, a linear underestimate can be obtained by extrapolation (see Figure 14b) of the time required to erode the entire valley. Only half the volume of sediment would have been displaced by the transport rate at the end of the experiment.

[51] In summary, this analysis shows that calculation of a formative duration based on the final slope overestimates the duration by about a factor of 2 for typical experimental

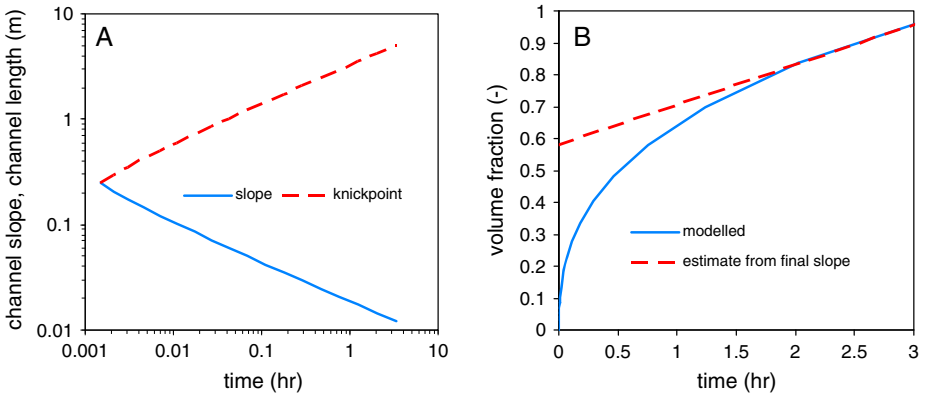


**Figure 14.** (A) Relaxation of slope over time and increase of knick point distance from the crater rim (which is the upstream channel length). (B) Normalized volume transported over time for the idealized scenario (Table 2) (1) showing a decline of delta volume growth rate as slope decreases over time. Extrapolation of the trend based on transport calculated for the final slope underestimates the deposit volume a factor of about 2 (intercept near 0.6).

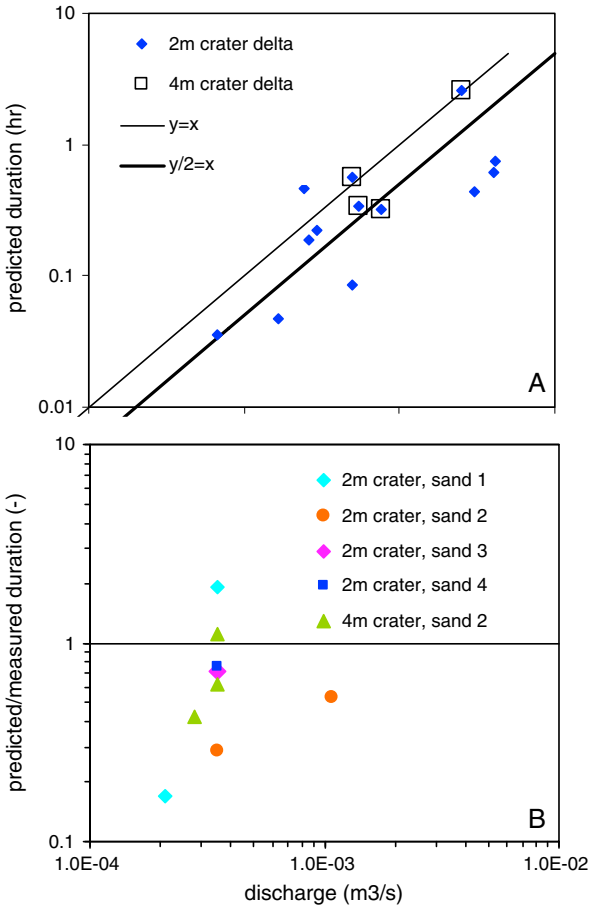


**Figure 15.** (A) Comparison of true and predicted event duration. Prediction is based on the measured delta volume divided by sediment transport rate predicted for the final slope. The line $y/2 = x$ shows perfect correspondence to represent possibilities that measured delta volume is underestimated with a factor of 2, or that sediment transport rate based on final slope underestimates the transported volume with a factor of 2. (B) Lack of relation between the discrepancy ratio (predicted/measured volume), discharge and particle size of the mixture $D_{90}$. The large crater experiments all have predictions within a factor of 2.5.

settings. This bias can be ascribed here to the large transport rates that occur over the initial steep slope from the channel into the crater as observed in our experiments. Furthermore the transport rate is the highest immediately after the connection between water source and impact crater basin causing hyperconcentrated flows. Such a flow forms a fan-shaped deposit akin to a mass flow dominated alluvial fan without a deltaic coastline, because the water table has not yet reached the deposit. This was also observed in the *Kraal et al*. [2008] experiments.

### 4.4. Back-Calculation of Sediment Transport Rate and Formative Duration

[52] The results of the experiments are interpreted based on the above analysis of appropriate flow and sediment transport predictors and the idealized model. First, the volume of the delta is calculated by subtraction of the initial DEM from the final DEM for the region of interest covering the recognizable delta. The predicted experiment duration that is required for the formation of a delta is referred to as event duration and can be calculated as the measured volume of the delta divided by the predicted sediment transport rate. The predicted event duration generally matches the measured event duration (Figure 15a). The formative duration of the delta is predicted within a factor of 3 for 8 out of 13 cases.

[53] The discrepancy ratio of predicted and measured formative duration is plotted in Figure 15a, where a ratio of unity implies perfect prediction. Experiments with low flow discharge may have lower discrepancy ratios because a significant proportion of the water is lost to the subsoil (Figure 9; see following section). Furthermore, poorly sorted sediment may form an amour layer on the channel bed surface [*Kleinhans and van Rijn*, 2002], which we indeed observed in experiments with the largest $D_{90}$ and poorest sorting. However, we found no significant relation between the discrepancy ratio, imposed flow discharge, and $D_{90}$ of the mixture (Figure 15b). For the smallest discharge the discrepancy ratios are indeed low for all sediments, except for the large crater experiments. We speculate that the small crater experiments have a relatively large volume of sediment to saturate below the channel and the crater rim, but this cannot be supported with observations.

[54] Prediction of sediment transport for experimental conditions of small water depth and relatively large bottom roughness are at most within a factor of 2 of the measured values, if measured under highly controlled conditions required for accurate flow shear stress determination. However, in cases where the final slope had to be used instead of a time-dependent slope for transport calculations, the shallow flow conditions may cause a factor of 10 uncertainty in transport rate.

### 4.5. Scaling Aspects

[55] Several scaling issues have to be addressed when experiments are used to interpret full-scale prototypes, in particular with reference to the difficulty of correctly scaling flow parameters, grain size, and basin floor permeability. Analysis of scaling between prototype and experiment serves to isolate experimental scale effects from phenomena that are expected to occur in nature as in the experiment, and to calculate possible mismatch between values of variables in prototype and experiment [*Cantelli et al*., 2004; *Kleinhans et al*., 2010b; *Lajeunesse et al*., 2010]. The most important variables are the dimensionless numbers characterizing essential aspects of flow and of sediment transport. These are the (1) Reynolds number for the flow, (2) the particle Reynolds number for the boundary layer of the flow, (3) the Shields mobility number, and (4) the Froude number [*Paola*, 2000; *van Heijst et al*., 2001; *Paola et al*., 2009].

[56] The Reynolds number of the flow assesses the occurrence of turbulence and is estimated as $Re = uh/\nu$ (−), where $u$ (m/s) is the flow velocity, $h$ (m) is the water depth and $\nu$ is the viscosity of water (here $1.6 \times 10^{-6}$ m$^2$/s). For $Re$ 500–2000, the flow is turbulent and for lower values of $Re$ it is laminar. Flow conditions inferred for Martian channels are always far above the transition to turbulence [*Kleinhans*, 2005], but in experimental channels $Re$ numbers are always low because of the limited flow depth. For a low estimate with $u \approx 0.15$ m/s and $h \approx 0.005$ m, the $Re \approx 750$, which is in the transitional regime. This may have reduced the

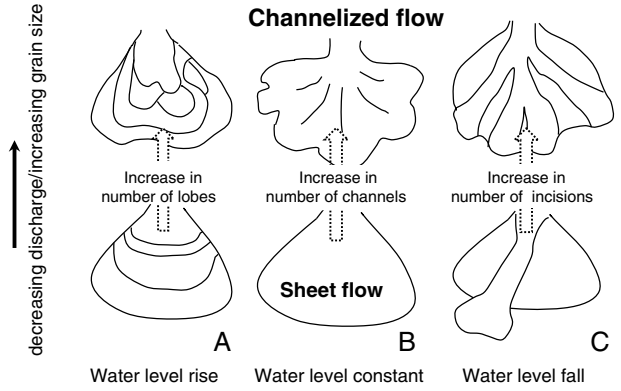


**Figure 16.** Three morphologically different types of delta deposits as a consequence of rising, steady, or falling water level (shown here on *x* axis). Subtypes of these deposits are formed based on the degree of channelization (shown here on *y* axis) as a consequence of variation in flow discharge and sediment texture.

tendency to suspend sediment but below we showed that mobility was well within ranges expected on Mars. Furthermore, *Lajeunesse et al*. [2010] argue in detail from the physics underlying channel and bar formation that turbulence is not important for the evolution of large-scale morphology in experiments.

[57] The particle Reynolds number characterizes the boundary layer of the flow. Hydraulically smooth conditions occur when the laminar sublayer at the bed is thicker than the particle size, which in our experiments (in water at about 10–20°C near the beginning of sediment motion) is the case for sediment of 0.5 mm diameter or smaller [*Kleinhans et al*., 2010a; *Lajeunesse et al*., 2010]. Hydraulic smooth conditions are conducive to the formation of unrealistically large scour holes and ripples. However, to ensure sediment mobility experiments require sediment as fine as possible without becoming cohesive, which happens for 0.06 mm or less. Our solution for the experiments described here was to use poorly sorted sand, where the small median diameter ensures high sediment mobility whilst the presence of larger particles (up to fine gravel) disrupts the laminar sublayer [*Kleinhans et al*., 2010a]. To assess the effect of different mixtures we varied sorting and also used fine sand as used in the *Kraal et al*. [2008] experiments. The Kraal-experiments indeed showed such unrealistic scour holes, but our present comparison show that this does not affect the general conclusions.

[58] The Shields number characterizes sediment mobility. This depends on the flow shear stress and the particle size. In the case of Martian systems, the flow conditions of the prototype are unknown and have to be inferred from final morphology and spatial context. The particle size is even more uncertain as it can hardly be seen on imagery due to resolution limitations and usually must be inferred from locations far away from the fans and deltas as landing sites are few and not necessarily located at or near or study sites. However, it is much larger than in most terrestrial systems that have been scaled to laboratory experiments and the scaling of the Martian fan deltas is therefore probably more optimal than for terrestrial deltas. Based on such limited observations and inferences, the mobility of many cases on Mars is in the transitional range between bed load dominated and suspended load dominated conditions [*Kleinhans et al*., 2010a]. This was calculated assuming the final channel slope to be representative. The experiments likewise show low mobility numbers between bed load and suspended load conditions. This fact independently confirms that the method is valid, because otherwise the mobility number would have been below the threshold for motion, which would not have led to channels and deltas, or high in the suspension regime, which could not have formed the Gilbertian profiles with lee sides up to the angle of repose. But the scenario calculation demonstrated that the mobility was much higher initially—high enough to initiate hyperconcentrated flow and upper stage plane bed conditions [see *Kleinhans*, 2005]. Given the similar range of mobility numbers of experiments and inferred prototype conditions, hyperconcentrated flows can also have occurred on Mars on the initially steep slopes. The sediment transport predictor used here for the high slopes is deemed appropriate to Mars [*Parsons and Nimmo*, 2010] because its concentrations approach that of granular avalanches at the angle of repose, and the angle of repose on Mars is not very different from that on Earth [*Kleinhans et al*., 2011].

[59] Flows in experimental channels like those in our experiments are generally turbulent and subcritical. With subcritical flow and self-forming rivers as feeder channels, exact Froude scaling was neither fully attainable nor necessary [*Postma et al*., 2008; *Kleinhans et al*., 2010a, 2010b]. Flow reconstruction in Martian channels indicates that at least in the final stages the flow is subcritical [*Kleinhans*, 2005]. We suspect flow into the Martian craters can well have been supercritical at first when the slope was much steeper. However, the evidence is mostly eroded so this cannot be verified from the presently known sites on Mars. In spite of scale effects in the hydraulics of flow, we maintain that these experiments are very suitable to explore large-scale morphological features and formative processes delta building, because landscape experiments reproduce these features so well [see also *Paola et al*., 2009]. Due to the observation that these types of laboratory examples show more dependence on boundary conditions and less dependence on actual sediment transport dynamics [*Postma et al*., 2008], the similarity of process approach [*Hooke*, 1968] was deemed sufficient for our experiments.

## 5. Discussion

[60] Our results show that the primary morphology of our experimental deltas is determined by the behavior of the water level in the basin, and that the secondary morphology is mainly determined by other variables such as flow discharge and particle size distribution. In Figure 16, we illustrate the two factors that dominate the morphology of these delta deposits: water level behavior (rising, constant and falling) and the main processes (flow discharge and sediment texture) that facilitate channelization. When there is channelization and not sheet flow, the degree to which the delta is channelized is a measure of bank stability, which is expressed by the amount of small channels on the delta surface. Low bank stability results in many short lived shallow depth channels (like on alluvial fan surfaces), while increasing bank stability results in a few single-thread channels [e.g., *Leopold and Wolman*, 1957]. In

the laboratory results the degree of channelization depends on the channel width relative to delta width and on the avulsion rate at the apex of the delta [see also *van Heijst and Postma*, 2001], which in turn are dependent on discharge, sediment texture, and basin size (which is directly related to the rate of water level rise/fall). These variables are all captured by the variable sediment mobility (see quantification section), which depends on flow discharge, grain size and channel slope.

### 5.1. Primary Morphology: Dependence on Water Level Behavior

[61] As stated above, the primary morphology of the experimental deltas is determined by water level behavior in the basin. The morphologically different types of deltas that were all formed under short period discharge conditions in the laboratory show remarkable resemblance to many of the delta deposits that have been described for Mars (i.e., compare Figure 1 to Figures 4–11; see *Cabrol and Grin* [1999], *Irwin et al*. 2005, *Di Achille et al*. [2006], *Kraal et al*. [2008], and *Hauber et al*. [2009]). The primary morphological features of both the laboratory and Martian deltas agree well with those of terrestrial deltas indicating that change of water level in the receiving basin is an important parameter [e.g., *Schumm et al*., 1987; *Postma*, 1990, 1995; *van Heijst and Postma*, 2001; *Postma*, 1995; *Muto and Steel*, 2004].

[62] Morphological features of Martian deltas, such as their stepped profiles, thus illustrate that water level history in the crater lake was dominant in determining delta shape. It means that catastrophic conditions and related rapid base level change in craters during delta formation played the dominant role in the shaping of the deltas, and that most deltas observed on Mars can form in one event (in agreement with *Kraal et al*. [2008]), simply because it is not possible to produce a stepped delta in more than one filling event without leaving some evidence of surface alteration by subsequent drainage, such as incisions or terraces (such as in experiment M).

[63] The *multiple foreset*, *stepped*, *retrograding delta* develops as a result of the rise in the water level (Figure 16a) and the decrease of transport capacity of the feeder channel with decreasing gradient. Back-stepping delta lobes have been described as a feature of water-level rise (a transgression shoreline by the original advocates of sequence stratigraphy, e.g., *Posamentier et al*. [1988], *van Wagoner et al*. [1988], *van Heijst et al*. [2001], and *Catuneanu et al*. [2009]).

[64] Auto-stepping has been described by *Muto and Steel* [1992, 1997] as an autocyclical process inherent to delta progradation onto a sloping basin floor during constant slow rise in water level that is responsible for stepped shorelines (also known as regression). The experiments by *Muto and Steel* [1992, 2001] were carried out with a constant rise in water level and a constant sediment supply. In experiments with independent base level control the sediment feed can be so high that stepped shorelines emerge without transgression of the water level. However, our experiments were conducted with a decreasing rate of water level rise that decreases due to the shape of the basin and a sediment supply that is not constant due to (1) the collapse of the upstream crater rim during the initial phases of the experiment, to (2) diminishing bank erosion due to widening of the feeder channel and decreasing flow velocity, and to (3) bank collapse in the upstream incising feeder channel as also observed by *Kraal et al*. [2008]. These two (constant rise in water level and constant sediment supply) factors are potentially responsible for a type of back-stepping that is strictly linked to the transgression of the water level. Thus, in our experiments and by inference on Mars, the sediment supply that is decreasing with time is not nearly sufficient to fill the new accommodation space that is generated by the rapidly rising water level, and thus promotes the back-stepping morphology.

[65] Major change in delta morphology, for instance from stepped fan to prograding fan, occurs only when the lake starts to spill over. For example, the *simple*, *single foreset*, *prograding delta* develops (Figure 16b) during the breaching of the crater wall, when the water level remains constant or is slowly falling. A *highly incised*, *telescopic*, *prograding delta* (Figure 16c) develops when the water level is rapidly falling (which occurs by down-cutting of the crater rim). The rate of falling of the water level is crucial in the formation of these two different types of deltas.

[66] A subtype of the prograding delta, the *branched*, *lobate-shaped*, *prograding delta* (also Figure 16b) is produced by reduced sediment mobility, thus in experiments with larger grain size and less well sorted sediment, or low discharge. Higher discharge maintains a more even delta plain surface because the runoff is sheet-flow dominated. Lower discharge results in more channelized flow on the delta surface, which causes more lobate-shaped delta fronts (Figure 16b). The depth and erosion rate of the breach would partly determine the water level, and the process is analogous to dike breaching and river bed erosion after dam removal [*de Villiers et al*., 2010] but is not further discussed here.

[67] The erosive power of the stream always ensured that the apex of the delta was below the original rim height. We expect step-like formations visible all the way into the feeder channel if the system was left to fill completely with water. In a few of our experiments we observed these steps retrograding all the way into the feeder channel. We never observed any step-like formations in the upstream feeder channels of the Martian deposits, and from this we infer that the Martian lakes may never have been entirely full when breaching occurred. In these few cases where the lowest part on the rim is at a higher elevation than the input stream, a breach was likely to form in the weakest part of the rim due to the pressure of the water in the lake against the rim rather than surface flow over the rim, which would not have been able to reach rim heights above that of the input stream. Numerous breached craters with both an inlet valley and an outlet valley, also known as “open basin lakes”, have been identified on the surface of Mars, with more than 200 described by *Fassett and Head* [2008].

### 5.2. Secondary Morphology: Dependence on Flow Discharge and Basin Characteristics

[68] An important aspect for the closed basin case considered here is that water level behavior is directly influenced by discharge and basin hypsometry, which is rarely the case on Earth. Geological principles developed for terrestrial deltas cannot directly be applied to Martian deltas because on Earth the ocean acts as an infinitely large basin relative to the river discharge, and the sea level is not much affected by river inflow. However, on Mars inflow is large relative to the basin size and the water level in the basin directly depends on the

discharge as well as on the basin hypsometry. Thus for Mars, we propose this strong relationship between upstream flow discharge, basin hypsometry, and water level behavior. This is in agreement with the results of *Kleinhans et al*. [2010a], who described a unique relation between delta shape and inflow discharge, given a basin hypsometry that determines the rate of lake level rise.

[69] The extent to which lake level behavior is influenced by discharge in closed impact crater basins also depends strongly on the permeability of the crater floor, because the relative loss of ponding water by infiltration is larger for the same final lake volume if the inflow rate is smaller. For Mars this permeability is largely unknown, but many impact craters were possibly quite permeable along the rim due to brecciation of the rock by the force of the impact itself, or due to earlier infilling of the crater by airfall fines or other fine material brought by aeolian transport [*French*, 1998]. Large unfilled faults and fractures could promote rapid loss of water from the crater basin, which would not lead to ponding and delta formation but alluvial fans instead. Low crater permeability is possible for craters with ice or water-rich saturated subsurfaces, and in such cases no alluvial fans are formed because immediate ponding will lead to rapid delta formation. We argue for the formation of most of the Martian deltas, especially those in large impact craters (diameter $>$ 5–10 km), by high discharge (catastrophic) aqueous events, thus providing enough water to fill even a somewhat permeable crater.

### 5.3. Secondary Morphology: Dependence on Sediment Texture

[70] The large grain-sizes of Sand 1 distribution in the experiments (Table 2) enhance the stability of bars and channels on the delta surface producing more lobate deltas, but it also dramatically reduces the mobility of the channels by static bed surface armoring. The smaller grain size distributions of Sands 2, 3, and 4 resulted in more sheet-flow and thus a less lobate delta shape. The degree of sorting of the sediment also plays a role in the morphology; a more well-sorted sediment resulted in less channelization and vice versa. The experiments with well-sorted sand revealed better developed steps in the back-stepping delta not only due to the higher mobility of the sediment but also due to the uniform nature of the grains. Poorly sorted sediment trapped the finer part of the sediment in the pore spaces before constructing the next step, resulting in less pronounced steps in the final morphology.

[71] The amount of fine silica flour enhanced the adhesive strength of the sediment causing somewhat more stable banks and narrower channels than in the cases without added fines. However, our experiments point out that addition of fines to the particle size distribution affects delta morphology only on a small scale leaving no detectable topographical signature in the lake [*de Villiers et al*., 2010]. This could be a partial explanation for the mismatch between eroded volume of channels and deposited volume of deltas observed on Mars [*Hauber et al*., 2009], where a fraction of the sediment (mainly fines) is likely to be carried away in suspension and not deposited on the delta but elsewhere in the system, further downstream. If the original percentage of fines in the sediment source is quite high, this could be a significant fraction of the sediment that is not trapped by the delta.

[72] The effects of different particle size distributions in the experiments point out that morphology of deltas depends partly on the smaller-scale morphodynamic processes such as channelization and sheet flow; however, the causes for these processes are only partly understood [*van Dijk et al*., 2009]. It may be that the smooth-topped deltas of Mars had sheet flow, or have channel dimensions beyond detection. Future high-resolution imagery may resolve questions on sediment sorting patterns and occurrence of small channels or sheet flows.

### 5.4. Implications for Mars

[73] We found three emergent properties of fan deltas formed in rapid discharge events that are generic and we infer them to be valid for Mars. First, an important observation in the experiments is the process of highly energetic hyperconcentrated flow in the early stages of the process. Some Martian deltas indeed show indications of having formed on top of another deposit that may have formed from a hyperconcentrated flow [*Kleinhans et al*., 2010a]. Second, all experiments confirm that incision is highly focused and occurs rapidly, so that deltas without obvious incisions must have formed in one event, or must have covered an earlier delta entirely which must, therefore, have been smaller. Third, the experiments indicated that the loss of water into the subsoil may lead to under-estimation of the total volume delivered by the source as inferred from formative duration and lake level indicators, particularly the shoreline. This was referred to as the "leaky cauldron hypothesis" in *Kleinhans et al*. [2010a]. However, the overall error due to this effect in the experiments is no more than of the order of a factor of two. As for the different permeabilities of the substrate, we are inclined to argue that the time of formation of delta deposits on Mars might be shortened due to the relatively smaller permeability of the sediment or bedrock when compared to our relatively coarse and unconsolidated laboratory sands.

[74] We conclude from the flume experiments and the numerical analyses that the most important dimensionless numbers governing behavior of flow and sediment are within reasonable or even narrow range of values inferred for Martian systems. The most important scale problem was crater rim incision because of the weak material and the narrow rim. The modeled crater rims were not only much more easily eroded, but were also narrower compared to natural craters [*Garvin and Frawley*, 1998], allowing the rim to be breached and eroded very rapidly. This caused many deltas in phase 2, the overflowing lake, to incise. This is not what we believe to be analogous to Martian conditions. On the contrary, we expect the crater rim on Mars to be substantially stronger and to resist rapid erosion and we expect the deltas to be much less incised. A much wider rim with a significant ejecta blanket simulated in the initial topography of the experiments would have largely reduced the incision processes that we observed on the deltas, particularly in the smaller craters.

[75] Interestingly, the calculations of the formative time scale in the experiments were only somewhat less uncertain than those on Mars. This is despite the much higher control on initial and boundary conditions, and likely due to the shallowness of the flow and the dramatic transition in sediment concentration which spanned hyperconcentrated flow to dilute flow.

### 5.5. Interpretation for Martian Climate

[76] On Earth, we rarely see examples of stepped deltas because receiving basins are very large compared to the volume of hydrological input. Contrastingly, on Mars, the development of the different delta types may have often been halted during the early phase of formation because the hydrological event ended. The ending was most likely very abrupt, because any lowering of lake level while there still was some upstream water supply would have led to erosion of the delta shoreline. Almost all deltas on Mars show no large-scale erosion by postformation flow over their surface (as also observed by *Irwin et al*. [2005]), with the possible exception of the deltas in Eberswalde and Jezero Craters and other similarly complex delta complexes [which are not the topic of discussion here, but have been discussed in more detail by *Malin and Edgett* [2003], *Fassett and Head* [2005], *Mangold et al*. [2012], and *Schon et al*. [2012]. The preservation of numerous deltas on Mars, mostly without indications of fluvial erosion, leads us to argue that the climate may not have been warm and wet and sustaining long-duration hydrological activity throughout Mars' history.

[77] More likely, from time to time, catastrophic events led to instant production of flood waters which rapidly filled crater basins. The hydrological events that were responsible for the delta formation ended abruptly and the crater lakes rapidly dried up, leaving the deltas exposed. The retrograding deltas on Mars are evidence of a hydrological event that ended soon after the rapid filling of the crater lake. The prograding deltas are evidence of a hydrological event that ended while the lake level was stable (either full or overflowing or slowly falling). This requires not only a trigger for initiation of flow, but also an explanation of the abrupt ending. Brief catastrophic events can be induced by heating of the groundwater or ground-ice in the subsurface for example through local volcanism or due to impact cratering [e.g., *Head and Wilson*, 2007; *Segura et al*., 2008]. Such processes will yield a short duration hydrological event, either through groundwater sapping or overland flow, or in exceptional cases, rainfall [*Kite et al*., 2011; *Jerolmack et al*., 2004; *Kleinhans*, 2005]. Sustained, continuous, or repeated events would imply a wet period for a longer time, on the order of a hundred thousand years or more, with the possibility of multiple aqueous events that must have had much larger effects on the morphology of sedimentary deposits than observed on Mars. In sequence stratigraphic terms [see *Catuneanu et al*., 2009], the occurrence of unaltered retrograding and prograding deltas on Mars indicates the formation of transgressive and high-stand deposits respectively, and the absence of incised deltas indicates that regressive and low-stand deposits were likely never formed. Unlike some authors [e.g., *Cabrol et al*., 2001; *Di Achille and Hynek*, 2010], we do not see evidence of cyclic discharges or a persistent hydrological cycle based on the morphologies or the mere occurrence of these deltas alone.

## 6. Conclusions

[78] The morphology of deltas formed in closed crater basins in the laboratory showed strong morphological resemblance of deltas in Martian craters. The morphologies of fan-shaped landforms on Mars and (dis)similarities with their counterparts on Earth and in the laboratory reflect upstream (i.e., flow discharge as well as sediment availability and mobility) and downstream (water level dynamics) conditions at the time of formation. Logical combinations of these conditions resulted in three main morphological delta types with variations in subtypes (Figure 16).

[79] The behavior of the downstream water level is the most important factor determining delta morphology. The main conditions to form the large-scale, primary delta morphology (1) stepped, retrograding delta, (2) smooth or branched, prograding delta, and (3) a telescopic, incised delta is by rising, steady or falling water level in the crater basin, respectively. Unlike in terrestrial cases, downstream conditions (rate of water level rise or fall) in the craters on Mars are entirely determined by upstream discharge, crater basin hypsometry, crater floor permeability, and the quality of the crater rim. Small-scale, secondary morphological features superimposed on the three main morphology types along the $x$ axis of Figure 16 depend on variations in flow discharge and sediment texture. Little evidence has been found for the highly incised, telescopic types of delta deposits on Mars, which leads us to propose that discharge onto the delta abruptly stopped before breaching of the crater rim and never resumed again (hence could not incise or erode the original deposit). Furthermore, breaching might not always have occurred, as subsurface drainage and evaporation may have been important factors that reduced water level rise until the upstream discharge was halted.

[80] Sediment transport rate is initially very high due to large amounts of available sediment in the upstream crater rim, implying the occurrence of "en-masse" sediment transport (mass flows) in the first formative stage of delta formation. The occurrence of mass flow events shortens the overall formative time scale because the majority of the sediment volume is rapidly deposited after which the sediment transport rate declines as the stream gradient decreases and the availability of sediment diminishes.

[81] Morphological evidence for episodic, short periods of intense hydrological activity is abundant and predominantly occurring in the craters of Mars. These events would flood the crater basin thus creating transgressive, retrograding delta deposits with multiple foresets. Some of these stepped deltas grew into prograding deltas with single foresets, prograding as lakes spilled over while maintaining a constant water level; however, most of these deltas do not show evidence for persistent hydrological activity. On the contrary, the smooth surfaces untouched by postformation fluvial erosion are evidence of the abrupt end of these short, episodic events. We therefore dismiss sustained water cycles as would occur by for example periods of wet climate (rainfall), which would result in more complex water level histories along with complex sediment delivery histories and delta morphologies. We therefore conclude that rapid formation by single, high discharge events was most likely responsible for most of these delta deposits on Mars.

[82] **Acknowledgments.** The authors would like to thank all anonymous reviewers for their assistance with improving this manuscript. We thank Ernst Hauber, Poppe de Boer, Steven de Jong and Wout van Dijk for discussion as well as Dimitri van Breemen and Jan de Vries for help with data collection. GdV was supported by the Netherlands Organisation for Scientific Research (NWO) (grant ALW-GO-PL/07-01 to MGK).

## References


Baker, V. (2001), Water and the Martian landscape, *Nature*, *412*(6843), 228–236.

Cabrol, N., and E. Grin (1999), Distribution, classification, and ages of Martian impact crater lakes, *Icarus*, *142*(1), 160–172.

Cabrol, N., and E. Grin (2001), The evolution of lacustrine environments on Mars: is Mars only hydrologically dormant?, *Icarus*, *149*(2), 291–328.

Cabrol, N., D. Wynn-Williams, D. Crawford, and E. Grin (2001), Recent aqueous environments in Martian impact craters: An astrobiological perspective, *Icarus*, *154*(1), 98–112.

Cantelli, A., C. Paola, and G. Parker (2004), Experiments on upstream-migrating erosional narrowing and widening of an incisional channel caused by dam removal, *Water Resour. Res.*, *40*, W03304.

Carr, M. (1983), Stability of streams and lakes on Mars, *Icarus*, *56*(3), 476–495.

Catuneanu, O. *et al*. (2009), Towards the standardization of sequence stratigraphy, *Earth Sci. Rev.*, *92*(1–2), 1–33.

Craddock, R. A., and A. D. Howard (2002), The case for rainfall on a warm, wet early Mars, *J. Geophys. Res.*, *107*(E11), 5111–5146.

de Villiers, G., M. G. Kleinhans, G. Postma, E. Hauber, S. de Jong, and P. L. de Boer (2009), Types of Martian Fan-shaped Sedimentary Deposits, *Lunar and Planet. Inst. Sci. Conf. Abstr.*, *40*, 1901.

de Villiers, G., M. G. Kleinhans, D. van Breemen, G. Postma, and E. Hauber (2010), Experiments on sedimentation in wide reservoirs and erosion following dam removal, *Proc. River Flow 2010 Conf.*, *2*, 1147–1154.

Di Achille, G., G. Ori, D. Reiss, E. Hauber, K. Gwinner, G. Michael, and G. Neukum (2006), A steep fan at Coprates Catena, Valles Marineris, Mars, as seen by HRSC data, *Geophys. Res. Lett.*, *33*(7), L07204.

Di Achille, G., and B. Hynek (2010), Ancient ocean on Mars supported by global distribution of deltas and valleys, *Nat. Geosci.*, *3*(7), 459–463.

Fassett, C. I., and J. W. Head (2005), Fluvial sedimentary deposits on Mars: Ancient deltas in a crater lake in the Nili Fossae region, *Geophys. Res. Lett.*, *32*, L14201. doi:10.1029/2005GL023456.

Fassett, C. I., and J. W. Head (2008), Valley network-fed, open-basin lakes on Mars: Distribution and implications for Noachian surface and subsurface hydrology, *Icarus*, *198*(1), 37–56.

Ferguson, R. (2007), Flow resistance equations for gravel- and boulder-bed streams, *Water Resoures Res.*, *43*. doi:10.1029/2006WR005422.

French, B. M. (1998), Traces of Catastrophe: A Handbook of Shock-Metamorphic Effects in Terrestrial Meteorite Impact Structures, *LPI Contrib.*, *954*, 120.

Gaidos, E., and G. Marion (2003), Geological and geochemical legacy of a cold early Mars, *J. Geophys. Res.*, *108*, 5055–5073.

Garvin, J., and J. Frawley (1998), Geometric properties of Martian impact craters: Preliminary results from the Mars Orbiter Laser Altimeter, *Geophys. Res. Lett.*, *25*(24), 4405–4408.

Garvin, J., S. Sakimoto, J. Frawley, and C. Schnetzler (2000), North polar region craterforms on Mars: Geometric characteristics from the Mars Orbiter Laser Altimeter, *Icarus*, *144*(2), 329–352.

Golombek, M., A. Haldemann, N. Forsberg-Taylor, E. DiMaggio, R. Schroeder, B. Jakosky, M. Mellon, and J. Matijevic (2003), Rock size-frequency distributions on Mars and implications for Mars Exploration Rover landing safety and operations, *J. Geophys. Res.*, *108*(E12), 8086–8108.

Grant, G. E. (1997), Critical flow constrains flow hydraulics in mobile-bed streams: a new hypothesis, *Water Resour. Res.*, *33*, 349–358.

Gulick, V. (2001), Origin of the valley networks on Mars: A hydrological perspective, *Geomorphology*, *37*(3–4), 241–268.

Hauber, E., K. Gwinner, M. G. Kleinhans, D. Reiss, G. Di Achille, G. Ori, F. Scholten, L. Marinangeli, R. Jaumann, and G. Neukum (2009), Sedimentary deposits in Xanthe Terra: Implications for the ancient climate on Mars, *Planetary and Space Science*, *57*(8–9), 944–957.

Head, J., and L. Wilson (2007), Heat transfer in volcanoice interactions on Mars: synthesis of environments and implications for processes and landforms, *Ann. Glaciol.*, *45*(1), 1–13.

Herkenhoff, K. E. *et al*. (2004), Textures of the soils and rocks at Gusev Crater from Spirit's microscopic imager, *Science*, *305*(5685), 824–826.

Hooke, R. (1968), Model geology: prototype and laboratory streams: discussion, *Bull. Geol. Soc. Am.*, *79*(3), 391–393.

Hynek, B., M. Beach, and M. Hoke (2010), Updated global map of Martian valley networks and implications for climate and hydrologic processes, *J. Geophys. Res.*, *115*(E9), E09008.

Irwin, R. I., A. Howard, R. Craddock, and J. Moore (2005), An intense terminal epoch of widespread fluvial activity on early Mars: 2. increased runoff and paleolake development, *J. Geophys. Res.*, *110*, E12S15.

Jerolmack, D. J., D. Mohrig, M. T. Zuber, and S. Byrne (2004), A minimum time for the formation of Holden Northeast fan, Mars, *J. Geophys. Res.*, *31*(21), L21701.

Kite, E. S., S. Rafkin, T. I. Michaels, and W. E. Dietrich (2011), Chaos terrain, storms, and past climate on Mars, *J. Geophys. Res.*, *116*, E10002.

Kleinhans, M. G., and L. C. van Rijn (2002), Stochastic prediction of sediment transport in sand-gravel bed rivers, *J. Hydraul. Eng.*, *128*(4), 412–425.

Kleinhans, M. G. (2005), Flow discharge and sediment transport models for estimating a minimum timescale of hydrological activity and channel and delta formation on mars, *J. Geophys. Res.*, *110*, 12003.

Kleinhans, M. G., H. van de Kasteele, and E. Hauber (2010a), Palaeoflow reconstruction from fan delta morphology on Mars, *Earth Planet. Sci. Lett.*, *294*(3–4), 378–392.

Kleinhans, M. G., W. van Dijk, W. van de Lageweg, R. Hoendervoogt, H. Markies, and F. Schuurman (2010b), From nature to lab: scaling self-formed meandering and braided rivers, *Proceedings of River Flow 2010 Conference*, 1001–1009.

Kleinhans, M. G., H. Markies, S. J. de Vet, A. C. in't Veld and F. N. Postema (2011), Static and dynamic angles of repose in loose granular materials under reduced gravity, *J. Geophys. Res. Planets*, *116*, E11004.

Kraal, E., E. Asphaug, J. Moore, and R. Lorenz (2006), Quantitative geomorphic modeling of Martian bedrock shorelines, *J. Geophys. Res.*, *111*(E3), E03001.

Kraal, E., M. van Dijk, G. Postma, and M. G. Kleinhans (2008), Martian stepped-delta formation by rapid water release, *Nature*, *451* (7181), 973–976.

Lajeunesse, E., L. Malverti, P. Lancien, L. Armstrong, F. Métivier, S. Coleman, C. E. Smith, T. Davies, A. Cantelli, and G. Parker (2010), Fluvial and submarine morphodynamics of laminar and near-laminar flows: a synthesis, *Sedimentology*, *57*, 1–26.

Leopold, L. B. and M. G. Wolman (1957), River Channel Patterns: Braided, Meandering and Straight, *Physiographic and Hydraulic Studies of Rivers*, *USGS Professional Paper* 282-B.

Malin, M., and K. Edgett (2003), Evidence for persistent flow and aqueous sedimentation on early Mars, *Science*, *302*(5652), 1931–1934.

Mangold, N., E. S. Kite, W. Dietrich, M. G. Kleinhans, H. Newsom, V. Ansan, E. Hauber, E. Kraal, C. Quantin, and K. Tanaka (2012), The origin and timing of fluvial activity at Eberswalde crater, Mars, *Icarus*, *220*(2), 530–551.

Melosh, J. (2011), *Planetary Surface Processes*, 520 pp., Cambridge University Press, New York.

Meyer-Peter, E. and R. Müller (1948), Formulas for bed-load transport, *Proceedings of the 2nd Meeting of the International Association for Hydraulic Structures Research*, 39–64.

Muto, T., and R. Steel (1992), Retreat of the front in a prograding delta, *Geology*, *20*(11), 967–970.

Muto, T., and R. Steel (1997), Principles of regression and transgression; the nature of the interplay between accommodation and sediment supply, *Journal of Sedimentary Research*, *67*(6), 994–1000.

Muto, T., and R. Steel (2001), Autostepping during the transgressive growth of deltas: Results from flume experiments, *Geology*, *29*(9), 771–774.

Muto, T., and R. Steel (2004), Autogenic response of fluvial deltas to steady sea-level fall: Implications from flume-tank experiments, *Geology*, *32*(5), 401–404.

Paola, C. (2000), Quantitative models of sedimentary basin filling, *Sedimentology*, *47*, 121–178.

Paola, C., K. Straub, D. Mohrig, and L. Reinhardt (2009), The "unreasonable effectiveness" of stratigraphic and geomorphic experiments, *Earth Sci. Rev.*, *97*, 1–43.

Parsons, R. A., and F. Nimmo (2010), Numerical modeling of Martian gully sediment transport: Testing the fluvial hypothesis, *J. Geophys. Res.*, *115*, E06001.

Porebski, S., and R. Steel (2006), Deltas and sea-level change, *J. Sediment. Res.*, *76*(3), 390–403.

Posamentier, H., M. Jervey, and P. Vail (1988), Eustatic controls on clastic deposition iconceptual framework, In: Sea-Level Changes: An Integrated Approach, *SEPM Spec. Publ.*, *42*, 109–124.

Postma, G. (1990), Depositional architecture and facies of river and fan deltas: a synthesis, In: Colella, A., and D.B. Prior (eds.), Coarse-Grained Deltas, *IAS Spec. Publ.*, *10*, 13–28.

Postma, G. (1995), Sea-level-related architectural trends in coarse-grained delta complexes, *Sediment. Geol.*, *98*(1–4), 3–12.

Postma, G. (2001), Physical climate signatures in shallow-and deep-water deltas, *Global Planet. Change*, *28*(1–4), 93–106.

Postma, G., M. G. Kleinhans, P. Meijer, and J. Eggenhuisen (2008), Sediment transport in analogue flume models compared with real-world sedimentary systems: A new look at scaling evolution of sedimentary systems in a flume, *Sedimentology*, *55*(6), 1541–1557.

Rickenmann, D. (1999), Empirical relationships for debris flows, *Nat. Hazards*, *19*, 47–77.

Ritchie, B., R. Gawthorpe, and S. Hardy (2004), Three-dimensional numerical modeling of deltaic depositional sequences 1: Influence of the rate and magnitude of sea-level change, *J. Sediment. Res.*, *74*(2), 203–220.

Schon, S. C., J. W. Head, and C. I. Fassett (2012), An overfilled lacustrine system and progradational delta in Jezero crater, Mars: Implications for Noachian climate, *Planet. Space Sci.*, *67*, 28–45.

Schumm, S. A., M. P. Mosley, and W. E. Weaver (1987), Experimental fluvial geomorphology, Wiley & Sons, New York, pp. 413 .

Segura, T., O. Toon, and A. Colaprete (2008), Modeling the environmental effects of moderate-sized impacts on Mars, *J. Geophys. Res.*, *113*(E11), E11007.

Smart, G. (1984), Sediment transport formula for steep channels, *J. Hydraul. Eng.*, *110*, 267–276.

Tye, R., and J. Coleman (1989), Depositional processes and stratigraphy of fluvially dominated lacustrine deltas; Mississippi delta plain, *J. Sediment. Res.*, *59*(6), 973–996.

Van Dijk, M., G. Postma, and M. G. Kleinhans (2009), Autocyclic behavior of fan deltas: an analogue experimental study, *Sedimentology*, *56*(5), 1569–1589.

Van Dijk, M., M. G. Kleinhans, G. Postma, and E. Kraal (2012), Contrasting morphodynamics in alluvial fans and fan deltas: effect of the downstream boundary, *Sedimentology*, *59*(7), 2125–2145.

Van Heijst, M., and G. Postma (2001), Fluvial response to sea-level changes: a quantitative analogue, experimental approach, *Basin Res.*, *13* (3), 269–292.

Van Heijst, M., G. Postma, X. Meijer, J. Snow, and J. Anderson (2001), Quantitative analogue flume-model study of river–shelf systems: principles and verification exemplified by the late quaternary colorado river–delta evolution, *Basin Res.*, *13*(3), 243–268.

Van Wagoner, J., H. Posamentier, R. Mitchum, P. Vail, J. Sarg, T. Loutit, and J. Hardenbol (1988), An overview of the fundamentals of sequence stratigraphy and key definitions, In: Sea-Level Changes: An Integrated Approach, *SEPM Spec. Publ.*, *42*, 39–45.

Wong, M., and G. Parker (2006), Reanalysis and correction of bed-load relation of Meyer-Peter and Müller using their own database, *J. Hydraul. Eng.*, *132*, 1159–1168.